45p

Technical Report No. 32-387

Calculation of Turbulent Boundary-Layer Growth and Heat Transfer in Axi-Symmetric Nozzles

David G. Elliott
Donald R. Bartz
Sidney Silver

jpl
JET PROPULSION LABORATORY
CALIFORNIA INSTITUTE OF TECHNOLOGY
PASADENA, CALIFORNIA

February 15, 1963

EB

NATIONAL AERONAUTICS AND SPACE ADMINISTRATION
CONTRACT NO. NAS 7-100

Technical Report No. 32-387

Calculation of Turbulent Boundary-Layer Growth and Heat Transfer in Axi-Symmetric Nozzles

David G. Elliott
Donald R. Bartz
Sidney Silver

D. R. Bartz, Chief
Propulsion Research Section

JET PROPULSION LABORATORY
CALIFORNIA INSTITUTE OF TECHNOLOGY
PASADENA, CALIFORNIA

February 15, 1963

CONTENTS

CONTENTS (Cont'd)

TABLES

FIGURES

FIGURES (Cont'd)

ABSTRACT

The method of Bartz (1954) for computing boundary-layer thicknesses, skin-friction, and heat flux in axi-symmetric nozzles has been revised and programmed for digital computer solution. The method solves, simultaneously, the integral momentum and energy equations for thin axi-symmetric boundary layers. Boundary-layer shape parameters are approximated from one-seventh power profiles of velocity and stagnation temperature, and skin-friction coefficient and Stanton number are evaluated as functions of boundary-layer thickness from the best available semi-empirical relations. An IBM 7090 program of the method is available.

I. INTRODUCTION

The prediction of local heat-transfer rates in rocket nozzles has been of vital concern since the advent of modern rocketry because of the importance of designing cooling systems which can successfully withstand the extreme environment. Initially, for want of better information on turbulent boundary layers in nozzles, the classic turbulent pipe-flow heat-transfer correlation equations of McAdams and of Colburn (Ref. 1) were applied by considering the nozzle flow to be a series of fully developed turbulent pipe flows. Each point in the nozzle was assumed to have been preceded by a very long pipe of the local diameter of interest. Because this approach seemed to work well (although there was a very limited amount of local heat-flux data with which to compare it), there was a tendency to lose sight of the fact that the flow was by no means fully developed; i.e., boundary layer extending to the flow axis of symmetry.

Unsatisfied with the apparent incompatibility of the actual flow regime with that which served as the basis for the analytical prediction, several workers attempted to solve the nozzle heat-transfer problem from a boundary-layer viewpoint making use of the integral momentum and energy equations (Ref. 2, 3). The essential difference between the nozzle problem and most of the turbulent boundary-layer analytical treatments then published was the necessity for retaining the pressure gradient terms in the equations of motion. The way was already partially paved since the momentum transfer problem had been successfully solved by approximate methods under the impetus of computing boundary-layer corrections to the contours of supersonic wind tunnel nozzles (Ref. 4, 5, 6).

The new extension achieved in References 2 and 3 was the handling of the heat transfer, as well as the

momentum transfer, problem. Numerical results from the approximate solutions obtained were found to agree reasonably well with limited experimental data then available, and with predictions made on the pipe flow basis except in nozzle entrance regions. Here the possibility of extremely thin boundary layers was shown to result in correspondingly high local heat fluxes, as should be expected. Armed with the conviction that the boundary-layer approach was physically valid, it was expected that this method of analysis would serve the purpose of making reasonably accurate predictions of convective heat transfer in rocket and other supersonic nozzles. It was expected that the analysis would be improved as further basic knowledge of the skin friction and heat transfer in accelerating turbulent boundary layers was obtained.

In that era, which preceded the wide availability of high-speed computers and the practice of sharing programs between organizations, it soon became evident that a method of analysis requiring the solution of a pair of differential equations with coefficients varying in accordance with each particular nozzle contour could not be used very widely. Consequently, a closed-form equation which could be hand-computed, and which closely approximated the results of the boundary-layer analysis for a particular typical nozzle configuration and typical initial boundary-layer conditions was sought and found. It was clearly evident from the boundary-layer heat-transfer calculations (Ref. 3) that the dominant parameter in the variation of the local heat-transfer coefficient was the local mass flux raised to the eight-tenths power. This suggested the possibility of again utilizing the dimensionless parameter approach employing Reynolds number, Prandtl number, and Nusselt number. This approach, however, raised the question of the characteristic length dimension to be used. A review of the boundary-layer development in a nozzle (Ref. 3, Fig. 3) showed that the local boundary-layer thickness varied in a systematic relationship with the local diameter, suggesting that the local diameter be used as the characteristic length. When the diameter was so employed, the dimensionless equation looked identical in form to the McAdams and Colburn pipe-flow equations with a proportionality constant to be determined, thus explaining, perhaps, the early success of such equations when applied to nozzle flow. The proportionality constant was determined by fitting the closed-form equation to the boundary-layer heat-transfer calculations at the throat for a particular case, estimated to be reasonably typical of current rocket nozzles. Some additional minor modifications resulting from variable properties considerations, and effects of throat radius of curvature, were deduced from the boundary-layer results and applied to the closed-form equation giving the result published in Ref. 7.

This closed-form equation served its purpose quite satisfactorily until, with time, several changes occurred. First, with the increasing availability of high-speed computers, the compromises inherent in such an equation were no longer necessary; an exact solution, to the extent permitted by knowledge of the turbulent boundary layer, could be computed almost as readily as the closed-form equation. Second, nozzles of interest were no longer restricted to simple conical convergent-divergent nozzles in which local flow conditions were easily expressible in terms of local area ratio. So-called "bell" nozzles resulted in regions of severely turned flow, in which the mass flux near the wall was considerably different from that predicted by one-dimensional calculations. Annular-throat nozzles of the "plug" type also raised the question of the applicable local diameter to be used in the closed-form equation. Third, the closed-form equation provided only heat-transfer coefficients, whereas the increased precision of rocket nozzle design made it desirable to know such boundary-layer parameters as the displacement and the momentum thicknesses. As shown later, these thicknesses permit computation of nozzle performance corrections and provide nozzle-contour corrections for calculations of the free-stream flow. Thus it appeared desirable to reformulate the turbulent boundary-layer heat-transfer equations in a form suitable to accommodate all of these new requirements, to eliminate compromises originally made to ease computational difficulties, and to program the result for digital-computer solution. At the same time, the analysis in Ref. 3 was re-examined in the light of new information and altered where it seemed advisable.

The Blasius skin-friction formula employed in Ref. 3 was replaced by Coles' correlation (Ref. 8) which better fits the data at high Reynolds and Mach numbers. Momentum thickness was made the characteristic dimension in computing the skin-friction coefficient since this thickness is a more fundamental property of the boundary layer than the velocity thickness employed in Ref. 3, and is the dimension employed in Coles' correlation. Energy thickness, with a correction for differing momentum thickness, was made the characteristic dimension in computing Stanton number, rather than velocity thickness with a correction for temperature thickness. Mach number was made an optional free-stream parameter to be prescribed in place of area ratio, facilitating application to nozzles of the bell and plug type. For convenience, axial distance, rather than distance along the wall, was made the position variable. Adiabatic recovery temperature, instead of stagnation temperature, was made the

driving potential in computing heat flux, improving accuracy at high Mach numbers, and provision was made for optionally employing enthalpy, rather than temperature, driving potential in cases where chemical reaction or variable specific heat must be considered. The momentum and static-temperature-distribution equations of Ref. 3 were corrected to apply more accurately to unequal momentum and energy thickness. Finally, a simultaneous, iterative, solution of the momentum and energy equations was formulated, rather than stopping at the first approximation as in Ref. 3.

Unfortunately, the intervening years have shed no light on the most important postulate of Ref. 3, that the skin friction and heat flux at any point in a nozzle are the same as they would be on a flat plate at the same free-stream conditions and boundary-layer thickness. Furthermore, as discussed later, the question of a variable-properties correction for severely cooled boundary layers has become clouded rather than clarified. Nevertheless, we believe we have attained, with the program described in this Report, the most generally applicable and precise method of computing nozzle boundary-layer growth and heat transfer possible within the limited knowledge now possessed.

The equations employed in the program are derived in the next Section. Instructions for utilizing the program, a sample case, comparisons with experiment, and a derivation of the effect of boundary-layer growth on rocket performance, are presented in subsequent sections. The equations and numerical procedures employed in the program are summarized in the Appendix.

A deck of the IBM 7090 program and input cards for the sample case can be obtained from the Technical Information Section, Jet Propulsion Laboratory.[1]

[1]Pasadena, California.

II. DERIVATION OF EQUATIONS

The basic scheme of the computation method derived in this Report is as follows:

1. Nozzle contour, free-stream conditions, wall temperatures, and initial boundary-layer thicknesses are specified.
2. Values are computed for the skin friction and heat flux that would occur on a flat plate at the nozzle inlet conditions.
3. Using these skin-friction and heat-flux values, the integral momentum and energy equations are employed to find the boundary-layer thicknesses at a second position a short distance downstream of the inlet, taking into account the changes in nozzle circumference, wall temperature, and free-stream conditions.
4. Steps 2 and 3 are repeated for the second nozzle position to find conditions at a third position, and the process is repeated until the end of the nozzle is reached.

The basis for computing the growth of the momentum and energy boundary-layer thicknesses is the simultaneous solution of the integral momentum and integral energy equations. These integral equations are usually derived either (1) from integration of the Prandtl boundary-layer equations with certain questionable assumptions made about the turbulent fluctuation correlation terms, or (2) from the control-volume viewpoint in which these turbulent fluctuation terms are ignored. The derivation presented here, although related to the second approach, differs by starting with the displacement-, momentum-, and energy boundary-layer thicknesses as basic definitions of the respective deficiencies in mass, momentum, and energy resulting from friction and heat transfer. This derivation is based on comparison of the real flow with a hypothetical adiabatic potential flow extending all the way to the wall, and having the same wall static-pressure distribution and total mass flux as the real flow. In the following treatment, the nomenclature employed for the real-flow and potential-flow nozzles will be introduced first, followed by the definitions of the

displacement, momentum, and energy thicknesses, a discussion of the assumptions employed, the derivation of the integral momentum and energy equations, the presentation of the skin-friction and heat-transfer correlation equations adopted, and the derivation of relations for the boundary-layer shape parameters linking the various thicknesses.

A. Nomenclature

1. Real Flow

Figure 1 presents the nomenclature for the real nozzle flow. The stagnation conditions of the gas flowing through the nozzle are: temperature T_0, pressure p_0, specific heat c_p, specific heat ratio γ, Prandtl number Pr, and viscosity μ_0. At a given station, the distance along the nozzle axis is z, the distance along the wall is x, the radius of the wall from the axis is r, the wall temperature is T_w, the retarding wall shear stress is τ_w, and the heat flux to the wall is q_w. At a distance y from the wall, the time-mean values of the turbulently fluctuating density, stagnation temperature, and x-component of the velocity are $\overline{\rho}$, $\overline{t}_0$, and $\overline{u}$, respectively. The velocity $\overline{u}$ varies from zero at the wall to the free-stream value U at distance δ from the wall; δ is the *velocity thickness* of the boundary layer. The stagnation temperature $\overline{t}_0$ varies from T_w at the wall to the free-stream value T_0 at distance Δ from the wall; Δ is the *temperature thickness* of the boundary layer.

There is a streamline of the flow, the nth streamline, which, for a finite distance upstream and downstream of station z, lies just beyond δ and Δ. Thus, all boundary-layer effects are confined between the nth streamline and the wall. At station z the nth streamline lies a distance δ'_r from the wall, and the gas flowing at that point has density ρ, pressure p, Mach number M, static temperature T, and viscosity μ. Although δ'_r is greater than both δ and Δ, the separation of these three points is assumed small enough that there is negligible difference in free-stream properties between them.

The fluxes of mass, momentum, and total enthalpy between the nth streamline and the wall for the real flow of Fig. 1 are $\dot{m}_r$ (lbm/sec), $\dot{M}_r$ (ft lbm/sec^2), and $\dot{H}_r$ (Btu/sec), respectively.

2. Potential Flow

Figure 2 presents the additional nomenclature required for describing the potential-flow nozzle in which the free-stream conditions U, ρ, and T_0, extend all the way to the wall. The nth streamline in the potential-flow nozzle is at identically the same location with respect to the nozzle axis as in the real-flow nozzle, but the wall must, in general, be at a different distance δ'_p from the nth

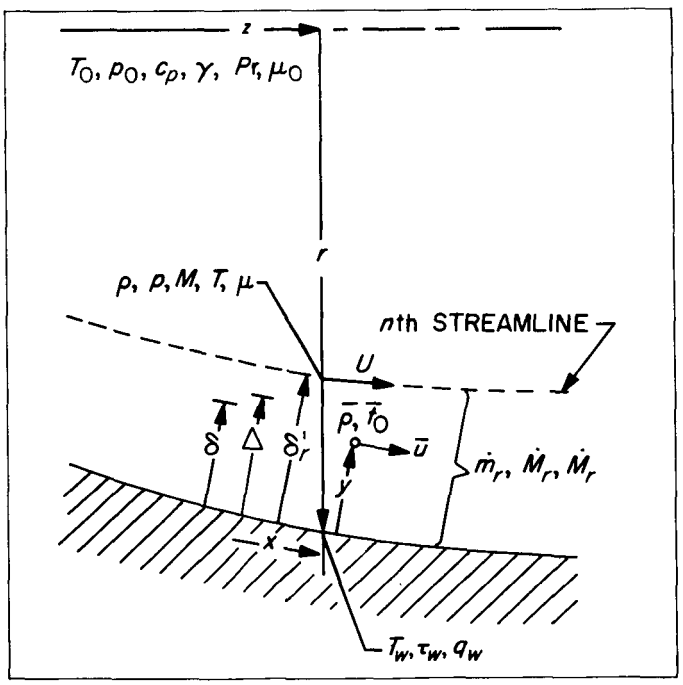

Fig. 1. Nomenclature for real flow

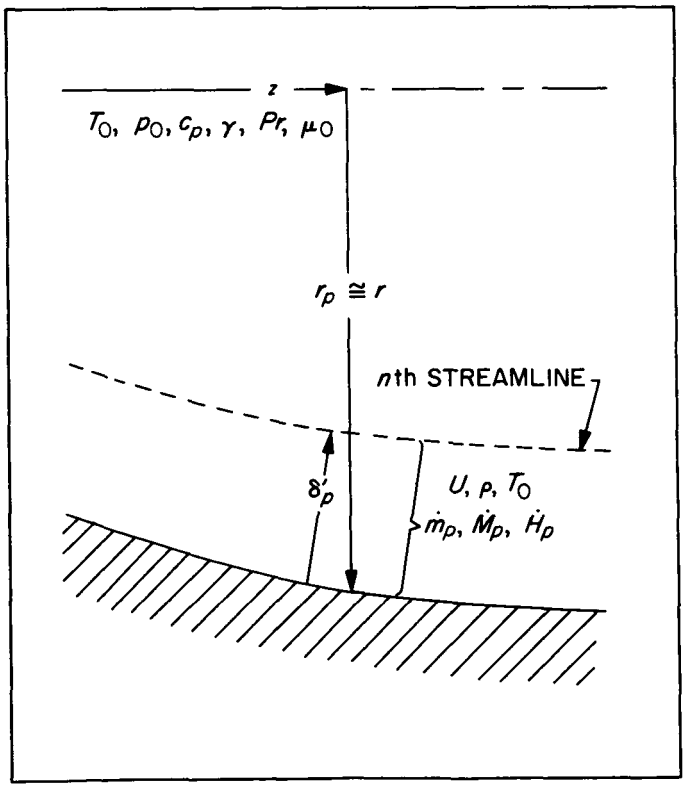

Fig. 2. Nomenclature for adiabatic potential flow

streamline in order for the mass flux $\dot{m}_p$ between that streamline and the wall to remain equal to $\dot{m}_r$. The momentum flux and enthalpy flux of $\dot{m}_p$ in the potential-flow nozzle are $\dot{M}_p$ and $\dot{H}_p$, respectively. Under the assumption that boundary-layer effects are confined to a small distance from the wall, relative to r, the wall radius r_p of the potential-flow nozzle is approximately equal to r.

B. Definitions

1. Deficiency Thicknesses

Under the assumption that δ_p' is small compared with r, it is seen from Fig. 2 that the fluxes of mass, momentum, and enthalpy (referenced to the wall temperature T_w) in the potential-flow nozzle are

$$\dot{m}_p = 2\pi r\rho U\delta_p' \tag{1}$$

$$\dot{M}_p = 2\pi r\rho U^2\delta_p' \tag{2}$$

$$\dot{H}_p = 2\pi r\rho U c_p (T_0 - T_w)\,\delta_p' \tag{3}$$

For δ_r' also small compared with r, it is seen from Fig. 1 that the fluxes of mass, momentum, and enthalpy in the real-flow case are, approximately,

$$\dot{m}_r \cong 2\pi r \int_0^{\delta_r'} \overline{\rho u}\, dy \tag{4}$$

$$\dot{M}_r \cong 2\pi r \int_0^{\delta_r'} \overline{\rho u^2}\, dy \tag{5}$$

$$\dot{H}_r \cong 2\pi r \int_0^{\delta_r'} \overline{\rho u} c_p (\bar{t}_0 - T_w)\, dy \tag{6}$$

Equations (4), (5), and (6) are approximate in that a product of mean values is not, in general, equal to the mean value of the product; the cross-correlation terms must be considered. For example, the product $\overline{\rho}\,\overline{u}$ in Eq. (4) is not necessarily equal to the time-mean flow density $\overline{\rho u}$ which would have to appear in Eq. (4) to make the equation exact. However, it can be argued that the cross-correlation terms substantially cancel out when the integration is performed over the boundary layer (Ref. 9, p. 1090).

Since δ_p' has been selected such that $\dot{m}_r = \dot{m}_p$, Eqs. (1) and (4) can be equated to yield the following expression for the difference in the wall positions between the two nozzles:

$$\delta_r' - \delta_p' = \int_0^{\delta_r'} \left(1 - \frac{\overline{\rho u}}{\rho U}\right) dy \tag{7}$$

The integral above is customarily defined as the *displacement thickness* δ^*. Thus, the physical significance of the displacement thickness is that δ^* *is the distance the wall must be moved inward for adiabatic potential flow as compared with the position of the wall for a real flow having the same mass flux*. That is, the physical definition of the displacement thickness is

$$\delta^* = \delta_r' - \delta_p' \tag{8}$$

while the integral definition is

$$\delta^* = \int_0^{\delta_r'} \left(1 - \frac{\overline{\rho u}}{\rho U}\right) dy \tag{9}$$

Because of the approximate nature of Eq. (7), resulting from the approximation in Eq. (4), Eqs. (8) and (9) do not define exactly the same quantity. The question of which definition to adopt as fundamental will be discussed later.

Subtracting Eq. (5) from Eq. (2) yields, with the aid of Eq. (7), the deficiency of momentum flux in the real flow as compared with the potential flow:

$$\dot{M}_p - \dot{M}_r = 2\pi r\rho U^2 \int_0^{\delta_r'} \frac{\overline{\rho u}}{\rho U}\left(1 - \frac{\bar{u}}{U}\right) dy \tag{10}$$

The integral above is customarily defined as the *momentum thickness* θ. Thus the physical significance of the momentum thickness is that θ *is the thickness of potential flow which has a momentum flux equal to that by which the momentum flux of the potential flow exceeds the momentum flux of the real flow for the same mass flux*. Hence, the physical definition of the momentum thickness is

$$\dot{M}_p - \dot{M}_r = 2\pi r\rho U^2\theta \tag{11}$$

and the integral definition is

$$\theta = \int_0^{\delta_r'} \frac{\overline{\rho u}}{\rho U}\left(1 - \frac{\bar{u}}{U}\right) dy \tag{12}$$

Subtracting Eq. (6) from Eq. (3) yields, with the aid of Eq. (7), the deficiency of enthalpy flux in the real flow as compared with the potential flow:

$$\dot{H}_p - \dot{H}_r = 2\pi r\rho U c_p (T_0 - T_w) \int_0^{\delta_r'} \frac{\overline{\rho u}}{\rho U}\left(1 - \frac{\bar{t}_0 - T_w}{T_0 - T_w}\right) dy \tag{13}$$

The integral above is customarily defined as the *energy thickness* ϕ. Thus the physical significance of the energy

thickness is that ϕ *is the thickness of potential flow which has an enthalpy flux equal to that by which the enthalpy flux of the potential flow exceeds the enthalpy flux of the real flow for the same mass flux.* Hence, the physical definition of the energy thickness is

$$\dot{H}_p - \dot{H}_r = 2\pi r \rho U c_p (T_0 - T_w)\phi \tag{14}$$

and the integral definition is

$$\phi = \int_0^{\delta_r'} \frac{\bar{\rho}\bar{u}}{\rho U}\left(1 - \frac{\bar{t}_0 - T_w}{T_0 - T_w}\right) dy \tag{15}$$

2. Coefficients

The skin-friction coefficient C_f is defined as the ratio of the wall shear stress to the free-stream dynamic pressure. Thus

$$C_f = \frac{2\tau_w}{\rho U^2} \tag{16}$$

The Stanton number C_h is defined as the ratio of the wall heat flux to the free-stream enthalpy flux based on the difference between adiabatic and actual wall temperature. Thus

$$C_h = \frac{q_w}{\rho U c_p (T_{aw} - T_w)} \tag{17}$$

The adiabatic wall temperature T_{aw} is the wall temperature for zero heat flux and is related to Mach number by

$$\frac{T_{aw}}{T_0} = \frac{1 + \frac{\gamma - 1}{2} RM^2}{1 + \frac{\gamma - 1}{2} M^2} \tag{18}$$

where R is the "adiabatic recovery factor."

C. Assumptions

The following assumptions are made in the analysis:

1. The flow is axi-symmetric and steady.
2. The boundary layer is confined to a distance from the wall which is small compared with the distance from the axis of symmetry.
3. The only forces acting on the gas are those due to pressure gradients and to skin friction at the wall.
4. The only changes in total enthalpy are those due to heat flux through the wall.
5. The flow immediately outside the boundary layer is isentropic and one-dimensional parallel to the wall.
6. Pressure is constant through the boundary layer perpendicular to the wall.
7. The gas follows the perfect gas law and has constant specific heats. (Optionally, the latter assumption can be removed in computing the driving potential for heat flux.)
8. The gas has a constant Prandtl number, a viscosity which varies as a power of the temperature, and an adiabatic recovery factor of 0.89 (that of air).
9. The skin-friction coefficient is the same as for constant-pressure constant-wall-temperature flow on a flat plate at the same free-stream conditions, wall temperature, and momentum thickness.
10. The Stanton number is the same as for constant-pressure constant-wall-temperature flow on a flat plate at the same free-stream conditions, wall temperature, energy thickness, and momentum thickness.
11. The Stanton number for unequal momentum and energy thicknesses is that for equal thicknesses multiplied by $(\phi/\theta)^n$, where n is a small "interaction exponent."
12. Heat transfer affects the skin-friction coefficient in one of two ways:
    a. There is no effect, and C_f is the same as for adiabatic flow, or
    b. C_f is the same as for adiabatic incompressible flow at a density and viscosity evaluated at the arithmetic mean between the actual wall temperature and the free-stream static temperature.
13. The Stanton number for equal momentum and energy thicknesses is related to the skin-friction coefficient by von Kármán's form of Reynolds' analogy.
14. Any chemical reactions in the boundary layer affect only the driving potential for heat flux.
15. The boundary-layer shape parameters θ/δ, Δ/δ, and δ^*/θ are those for 1/7-power profiles of velocity and of the difference between stagnation and wall temperature.

Assumptions 1, 2, 3, and 4 define the situation to which the analysis applies. Assumption 3 excludes, for example, magnetohydrodynamic forces, and Assumption 4 excludes combustion effects (except for a possible direct effect on heat flux as allowed by Assumption 14). Assumptions 1 and 2 have already been employed in defining δ^*, θ,

and ϕ. Assumptions 5 and 6 are good approximations if the flow has no strong shocks. Assumptions 7 and 8 introduce little error for most gases.

Assumptions 9 and 10 are the ones which most affect the results, and they are also the most uncertain. That skin friction and heat flux have the flat-plate dependence on local conditions is certainly valid asymptotically for gradual nozzle contours ($dr/dz \to 0$ and $dT_w/dz \to 0$), but the extent of departure in practical nozzles remains unexplored by experiment except for the limited data of Ref. 10 which tend to support the present assumption. The second area of uncertainty is the boundary-layer thickness to be used in correlating with flat-plate conditions. Excluding δ and Δ as vaguely defined and δ^* as not directly related to skin friction and heat flux, the most appropriate boundary-layer thicknesses for correlating with flat-plate conditions appear to be the momentum thickness θ for correlating skin friction and the energy thickness ϕ for correlating heat flux, since skin friction cannot depend very much on ϕ or heat flux on θ. However, a momentum thickness smaller than energy thickness might have a secondary effect on heat flux by moving the region of maximum turbulence closer to the wall, increasing heat flux by some factor such as that postulated in Assumption 11; the interaction exponent n is not known, but, as discussed later, can be no greater than 0.25 and is probably about 0.1, making the results relatively insensitive to its choice.

Assumption 12 has two options, either of which can be selected in the computer program. Assumption 12a is based on recent experiments (Refs. 11, 12, 13, and 14) which showed no measurable effect of heat transfer on skin-friction coefficient or Stanton number for cooled boundary layers. Assumption 12b is the widely-used procedure of evaluating properties at a "film" temperature and gives only slightly different values of C_f from those determined by the "reference" temperature method (Ref. 15) out to Mach numbers of interest for most nozzle flows. However, the background of data on which the "film" or "reference" methods were established for the cooled turbulent case is sketchy, consisting mainly of data with negligible temperature differences, i.e., T_w/T_0 only slightly less than unity, on average data over long pipe lengths in which uncertain axial-property variations clouded the picture considerably, and data which generally scattered to the same extent as the magnitude of the variable properties corrections. Neither of the classical references, 16 and 17, nor any of the more recent related references 18, 19, and 20, presented data which could definitively answer the question of the validity of the "film" or "reference" methods of variable-properties correction for severely cooled turbulent boundary layers. In the authors' opinion the adoption of these methods of variable properties correction for cooling was based more on their apparent validity for high-speed adiabatic flow and for heating, and their agreement with theoretical analyses (Ref. 21 and 22), than on specific data. Faced with the quandary of having doubt thrown upon the variable-properties correction by the new data and yet not being fully convinced that there should be *no* correction on the basis of the limited data cited, the authors chose to throw the burden of decision on the program user by making provision for either including or omitting the "film temperature" correction for variable properties.

Assumption 13 is well substantiated by experiment, as will be shown later. Assumption 14 represents the computationally convenient viewpoint that the effect of chemical recombination can be accounted for by employing enthalpy (rather than temperature) driving potential, leaving the heat-transfer coefficient unaltered. Assumption 15 agrees roughly with observed velocity and temperature profiles on flat plates and wind-tunnel nozzles, and the resulting values computed for δ and Δ are likewise rough approximations. However, the only effect of Assumption 15 on the other parameters computed is through the ratio δ^*/θ which is relatively insensitive to the profiles assumed, and which, in turn, has only a secondary effect on momentum thickness and skin friction, and little or no effect on energy thickness and heat flux.

D. Integral Equations

The usual approach to the derivation of the integral momentum and energy equations for a turbulent boundary layer (Refs. 3 and 9) is to start with the boundary-layer differential equations and introduce an approximation by eliminating the fluctuating cross-correlation terms through arguments that they substantially cancel out when integrated across the boundary layer (Ref. 9, p. 1090). Through this process one arrives at integrals of time-averaged variables such as

$$\int_0^{\delta_r'} \left(1 - \frac{\bar{\rho}\bar{u}}{\rho U}\right) dy$$

which are then defined as exactly equal to new variables δ^*, θ, and ϕ. In this case the definitions given by Eqs. (9), (12), and (15) are considered fundamental. However, the variables δ^*, θ, and ϕ are then related only approximately to the physical mass, momentum and energy defects, and the resulting momentum and energy equations become approximations of uncertain accuracy when written in terms of these integrally defined variables.

An alternate derivation of the integral momentum and energy equations, which will be presented here, adopts at the outset the physical definitions of δ^*, θ, and ϕ given, respectively, by Eqs. (8), (11), and (14). It will be seen that this approach leads directly to the integral momentum and energy equations without approximation and without consideration of the internal structure of the boundary layer. The resulting equations are identical in appearance with those derived from the differential equations, differing only in the definitions associated with δ^*, θ, and ϕ. In the authors' opinion, the present method is more direct and logical. However, the uncertainty in the integral expressions for δ^*, θ, and ϕ due to the turbulent fluctuation terms still affects the results, to a minor extent, through the use of the integral expressions in the shape parameters introduced later, and in evaluating Reynolds numbers in most of the available skin-friction data.

1. Momentum Equation

For the wall flow $\dot{m}_p$ without friction, the streamwise gradient of momentum flux $\dot{M}_p$ is, by Assumption 3, balanced only by the pressure gradient acting over the flow area $2\pi r\delta_p'$, where the latter, from the physical definition of the displacement thickness, Eq. (8), is equal to $2\pi r(\delta_r' - \delta^*)$. Thus, employing the physical definition of the momentum thickness from Eq. (11), the momentum-flux gradient is

$$\frac{d}{dx}(\dot{M}_r + 2\pi r\rho U^2\theta) = -2\pi r(\delta_r' - \delta^*)\frac{dp}{dx} \tag{19}$$

For the real wall flow $\dot{m}_r$, the streamwise gradient of momentum flux $\dot{M}_r$ is balanced by both the wall shear force and the pressure gradient acting over the area $2\pi r\delta_r'$. Thus

$$\frac{d}{dx}\dot{M}_r = -2\pi r\tau_w - 2\pi r\delta_r'\frac{dp}{dx} \tag{20}$$

Subtracting Eq. (20) from Eq. (19), and noting that by Assumptions 5 and 7 $dp/dx = -\rho U\,dU/dx$, the following relation is obtained:

$$\frac{d}{dx}(r\rho U^2\theta) = r\tau_w - r\rho U\delta^*\frac{dU}{dx} \tag{21}$$

Equation (21) is the integral momentum equation for thin axi-symmetric boundary layers. It can be put in a more convenient form by differentiating by parts, introducing the definition of the skin-friction coefficient, Eq. (16), and rearranging to give

$$\frac{d\theta}{dx} = \frac{C_f}{2} - \theta\left[\frac{1 + \delta^*/\theta}{U}\frac{dU}{dx} + \frac{1}{\rho U}\frac{d(\rho U)}{dx} + \frac{1}{r}\frac{dr}{dx}\right] \tag{22}$$

Under Assumptions 5 and 7 the expressions involving ρ and U can be written in terms of the Mach number M as follows:

$$\frac{1}{U}\frac{dU}{dx} = \frac{1}{M\left(1 + \frac{\gamma - 1}{2}M^2\right)}\frac{dM}{dx} \tag{23}$$

$$\frac{1}{\rho U}\frac{d(\rho U)}{dx} = \frac{1 - M^2}{M\left(1 + \frac{\gamma - 1}{2}M^2\right)}\frac{dM}{dx} \tag{24}$$

Substituting these expressions into Eq. (22) and transforming the independent variable to z by noting that $dx/dz = [1 + (dr/dz)^2]^{1/2}$, the final form of the integral momentum equation is obtained:

$$\frac{d\theta}{dz} = \frac{C_f}{2}\left[1 + \left(\frac{dr}{dz}\right)^2\right]^{1/2} - \theta\left[\frac{2 - M^2 + \frac{\delta^*}{\theta}}{M\left(1 + \frac{\gamma - 1}{2}M^2\right)}\frac{dM}{dz} + \frac{1}{r}\frac{dr}{dz}\right] \tag{25}$$

2. Energy Equation

For the wall flow $\dot{m}_p$ without heat transfer, the enthalpy flux, by Assumption 4, remains constant. Thus, employing the physical definition of the energy thickness from Eq. (14), the streamwise gradient of the enthalpy-flux $\dot{H}_p$ is

$$\frac{d}{dx}[\dot{H}_r + 2\pi r\rho U c_p(T_0 - T_w)\phi] = 0 \tag{26}$$

For the real wall flow $\dot{m}_r$, the streamwise gradient of the enthalpy flux $\dot{H}_r$ is exactly equal to minus the rate at which energy is transferred to the wall. Thus

$$\frac{d}{dx}\dot{H}_r = -2\pi r q_w \tag{27}$$

Subtracting Eq. (27) from Eq. (26) yields

$$\frac{d}{dx}[r\rho U c_p(T_0 - T_w)\phi] = r q_w \tag{28}$$

Equation (28) is the integral energy equation for thin axi-symmetric boundary layers. It can be put in a more convenient form by differentiating by parts, introducing the definition of the Stanton number, Eq. (17), and rearranging to give

$$\frac{d\phi}{dx} = C_h\left(\frac{T_{aw} - T_w}{T_0 - T_w}\right) - \phi\left[\frac{1}{\rho U}\frac{d(\rho U)}{dx} + \frac{1}{r}\frac{dr}{dx} - \frac{1}{T_0 - T_w}\frac{dT_w}{dx}\right] \tag{29}$$

Substituting Eqs. (23) and (24) and transforming the independent variable to z yields the final form of the integral energy equation

$$\frac{d\phi}{dz} = C_h\left(\frac{T_{aw} - T_w}{T_0 - T_w}\right)\left[1 + \left(\frac{dr}{dz}\right)^2\right]^{1/2} - \phi\left[\frac{1 - M^2}{M\left(1 + \frac{\gamma - 1}{2}M^2\right)}\frac{dM}{dz} + \frac{1}{r}\frac{dr}{dz} - \frac{1}{T_0 - T_w}\frac{dT_w}{dz}\right] \tag{30}$$

E. Skin-Friction Coefficient

1. Diabatic Skin-Friction Coefficient

In accordance with Assumption 9, the skin-friction coefficient in a nozzle is taken to be the same as that on a flat plate at the same free-stream conditions, ρ, U, μ, T_0, and M, same wall temperature T_w, and same momentum thickness θ. Unfortunately, even this drastic assumption does not permit a completely reliable evaluation of C_f, since only the *adiabatic* skin-friction coefficient C_{f_a}, obtained when $T_w = T_{aw}$, is known accurately. The relationship between C_f and C_{f_a} for severely cooled turbulent boundary layers, when gas properties vary greatly between the free stream and the wall, is sufficiently uncertain that both relationships discussed earlier have been programmed and the choice left to the user. The first relationship, Assumption 12a, is that of computing the value of C_{f_a} corresponding to the free-stream gas properties and assuming that this is equal to C_f.

$$\frac{C_f}{C_{f_a}} = 1 \tag{31-a}$$

The second relationship, Assumption 12b, is that of computing the effect of variable properties on skin friction, due either to heat transfer or compressibility, by evaluating the gas properties at the arithmetic-mean temperature between T and T_w. That relationship was employed in Ref. 3. Dividing Eq. (16) of Ref. 3 by Eq. (15) of Ref. 3, the film-temperature correction to the low-speed value of C_{f_a} (denoted by $\bar{C}_f$), is[2]

$$\frac{C_f}{\bar{C}_f} = \frac{1}{\left[\frac{1}{2}\left(\frac{T_w}{T} + 1\right)\right]^{(3-m)/4}} \tag{31-b}$$

where m is the exponent of the temperature dependence of viscosity which, according to Assumption 8, varies as

$$\frac{\mu}{\mu_0} = \left(\frac{T}{T_0}\right)^m \tag{32}$$

The limited available data cast doubt on Eq. (31-b) for cooling of the boundary layer. The only known measurement of the effect of heat transfer on skin friction in high-speed flow is that of Ref. 11 at $M = 5.0$ and 6.8 which showed no effect of cooling or, at most, a slight effect opposite that predicted by Eq. (31-b). Furthermore, as discussed earlier, the validity of Eq. (31-b) is in doubt for low-speed flow as well. Equation (31-b) is included as an option in the computer program to provide continuity with Ref. 3 and give the benefit of doubt to earlier data, but the authors recommend the use of Eq. (31-a) as representing the best current information.

2. Adiabatic Skin-Friction Coefficient

The most accurate method for computing the adiabatic skin-friction coefficient C_{f_a} is judged to be that of Coles (Ref. 8). Coles employs a transformation method which gives C_{f_a} as a function of Mach number M and the momentum-thickness Reynolds number R_θ defined by

$$R_\theta = \frac{\rho U \theta}{\mu} \tag{33}$$

Employing Eq. (32), R_θ can be written

$$R_\theta = \frac{\rho U \theta}{\mu_0}\left(\frac{T_0}{T}\right)^m \tag{34}$$

where, by Assumptions 5 and 7,

$$\frac{T_0}{T} = 1 + \frac{\gamma - 1}{2}M^2 \tag{35}$$

and

$$\rho U = \frac{\gamma p_0 M}{[c_p T_0 (\gamma - 1)]^{1/2}\left(1 + \frac{\gamma - 1}{2}M^2\right)^{\frac{\gamma+1}{2(\gamma-1)}}} \tag{36}$$

[2]The values of $C_f/\bar{C}_f$ computed on this basis differ by less than 10% from those computed on the "reference enthalpy" basis, Ref. 15, out to Mach 4.0.

Coles shows that the available data on the variation of C_{f_a} with R_θ and M can be correlated within a few per cent by a single curve of

$$\bar{C}_f = \frac{\rho\mu_s}{\rho_{aw}\mu_{aw}} C_{f_a} \tag{37}$$

as a function of

$$\bar{C}_f \bar{R}_{\bar{\theta}} = \frac{\rho\mu}{\rho_{aw}\mu_{aw}} C_{f_a} R_\theta \tag{38}$$

where ρ_{aw} and μ_{aw} are the density and viscosity evaluated at T_{aw} and μ_s is the viscosity at a mean "sublayer" temperature T_s given by

$$\frac{T_s}{T_{aw}} = 1 + 17.2\left(\frac{T_o}{T_{aw}} - 1\right)\left(\frac{\bar{C}_f}{2}\right)^{1/2} - 305\left(\frac{T_o}{T_{aw}} - \frac{T}{T_{aw}}\right)\frac{\bar{C}_f}{2} \tag{39}$$

It is seen that $\bar{C}_f$ and $\bar{R}_{\bar{\theta}}$ are merely the values of C_{f_a} and R_θ for low-speed flow. Coles' relation between $\bar{C}_f$ and $\bar{C}_f \bar{R}_{\bar{\theta}}$ is shown in Fig. 3. The circled points are values tabulated in Ref. 8 (p. 65) and are reproduced in Table 1. For values of $\bar{C}_f \bar{R}_{\bar{\theta}}$ above 64.8, the relation employed is the asymptotic one given by Eqs. (A-3) and (A-7) of Ref. 8 combined to yield

$$\left(\frac{2}{\bar{C}_f}\right)^{1/2} = 2.44 \ln\left[\frac{(\bar{C}_f \bar{R}_{\bar{\theta}})}{\bar{C}_f\left(3.781 - \frac{25.104}{\left(\frac{2}{\bar{C}_f}\right)^{1/2}}\right)}\right] + 7.68 \tag{40}$$

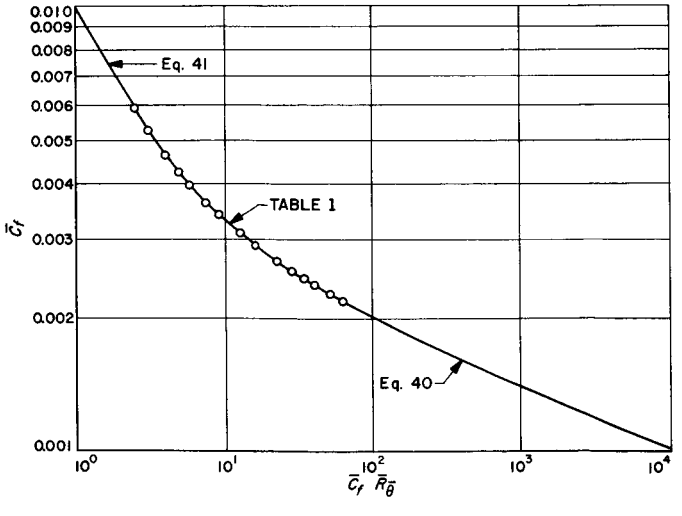

Fig. 3. Adiabatic skin-friction coefficient for low-speed flow

Table 1. The local friction law for the turbulent boundary layer at constant pressure[1]

$\bar{C}_f \bar{R}_{\bar{\theta}}$	$\bar{C}_f$
2.51	0.00590
3.10	0.00524
3.97	0.00464
4.88	0.00426
5.73	0.00398
7.41	0.00363
8.94	0.00340
12.75	0.00308
16.36	0.00290
23.2	0.00269
29.6	0.00255
35.9	0.00246
41.8	0.00238
53.6	0.00227
64.8	0.00219

[1]From Ref. 8.

To permit choice of small initial boundary-layer thicknesses, Table 1 is extended below $\bar{C}_f \bar{R}_{\bar{\theta}} = 2.51$ by

$$\bar{C}_f = \frac{0.009896}{(\bar{C}_f \bar{R}_{\bar{\theta}})^{0.562}} \tag{41}$$

The corresponding Reynolds numbers are below the region of turbulent flow and results for this region, and for the lower Reynolds numbers in Table 1, must be considered merely order-of-magnitude approximations.

Values of $\bar{C}_f$ for the film-temperature calculation of C_f (Eq. 31-b) are obtained directly from Eqs. (40) and (41) and Table 1 by setting $\bar{R}_{\bar{\theta}} = R_\theta$. The Blasius formula employed for computing $\bar{C}_f$ in Ref. 3 agrees with these values within 5% from $R_\theta = 400$ to $R_\theta = 15{,}000$.

Writing density and viscosity in terms of temperature, Eqs. (37) and (38) become

$$C_{f_a} = \frac{\bar{C}_f}{\left(\frac{T_{aw}}{T}\right)\left(\frac{T_s}{T_{aw}}\right)^m} \tag{42}$$

and

$$\bar{C}_f \bar{R}_{\bar{\theta}} = \left(\frac{T_{aw}}{T}\right)^{1-m} C_{f_a} R_\theta \tag{43}$$

F. Stanton Number

By Assumption 10 the Stanton number in a nozzle is taken to be the same as that on a flat plate at the same free-stream conditions ρ, U, μ, T_0, M, same wall temperature T_w, and same energy and momentum thicknesses ϕ and θ.

The most accurate available relation for computing flat-plate Stanton number is von Kármán's form of Reynolds' analogy (Ref. 23, p. 225) which relates Stanton number to skin-friction coefficient, with a secondary correction for non-unity Prandtl number, as follows:

$$C_h = \frac{\frac{C_f}{2}}{1 - 5\left(\frac{C_f}{2}\right)^{\frac{1}{2}}\left[1 - Pr + \ln\left(\frac{6}{5\,Pr + 1}\right)\right]} \tag{44}$$

By Assumption 13, Eq. (44) applies when the momentum and energy thicknesses are equal, $\theta = \phi$. Under the same circumstances $R_\theta = R_\phi$, where R_ϕ is the energy-thickness Reynolds number defined by

$$R_\phi = \frac{\rho U \phi}{\mu} \tag{45}$$

If R_ϕ is employed instead of R_θ in the procedure described in the preceding section for computing skin-friction coefficient, a number is obtained which is designated $C_f(R_\phi)$. If $\phi = \theta$, then $C_f(R_\phi) = C_f$, and the Stanton number in this special case is

$$C_h = \frac{\frac{C_f(R_\phi)}{2}}{1 - 5\left(\frac{C_f(R_\phi)}{2}\right)^{\frac{1}{2}}\left[1 - Pr + \ln\left(\frac{6}{5\,Pr + 1}\right)\right]} \tag{46}$$

Since C_h clearly must depend more on ϕ than on θ (in particular, C_h must approach infinity as ϕ approaches zero, regardless of the value of θ), Eq. (46) is taken as the first approximation to C_h for *unequal* θ and ϕ as well.

Equation (46), evaluated for $Pr = 0.7$ (air), is compared in Fig. 4 with a representative portion of each of the two sets of Stanton-number data believed to be the best available for flat-plate and tube-entrance flow. Reynolds, Kay, and Kline (Ref. 12) present values of C_h for flat-plate flow as a function of Reynolds number based on distance x from the start of turbulent flow; for present purposes these Reynolds numbers were multiplied by ϕ/x to obtain R_ϕ, ϕ being computed from the low-speed flat-plate energy equation (Eq. 30 for $z = x$, $T_0 = T_{aw}$, $dM/dx = dr/dx = dT_w/dx = 0$)

$$\phi = \int_0^x C_h\, dx$$

Wolf (Ref. 13) presents values of heat transferred in successive separately-cooled sections of a tube entrance from which values of ϕ have been computed at the end of each section and C_h obtained by differentiation, $C_h = d\phi/dx$; free-stream properties were taken to be those at the tube axis and computations were made only for the undeveloped entrance flow, where a reasonable simulation of flat-plate flow exists.

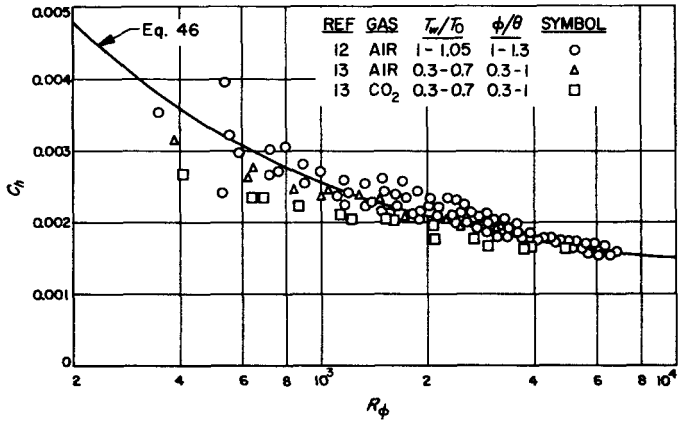

Fig. 4. Comparison of theoretical and experimental Stanton number for low-speed flow

It can be seen from Fig. 4 that both sets of data fall, for the most part, within ±15% of Eq. (46). This agreement is to be expected for the data of Ref. 12, since the near-unity ratios of T_w/T_0 and ϕ/θ are the conditions on which the equation is based. The agreement of Eq. (46) with the data of Ref. 13, however, is remarkable in that the data points correspond to temperature ratios T_w/T_0 ranging from 0.3 to 0.7 (for different tests) and boundary-layer thickness ratios ϕ/θ ranging from 0.3 to 1.0 (for successive cooled sections, the velocity boundary layer being fully developed at the test-section entrance). It is the data of Ref. 13 which are the strongest evidence that Stanton number and skin-friction coefficient are insensitive to T_w/T_0 for cooling, as expressed in Eq. (31-a).

It is seen from Fig. 4 that the effect of non-unity ϕ/θ cannot be large for $\phi < \theta$. However, the scatter of the data could mask a small effect, and the case usually occurring in nozzles is $\phi > \theta$, which could have a larger effect. To allow for such possibilities, the final equation for C_h employed in the program is Eq. (46) multiplied, in accordance with Assumption 11, by $(\phi/\theta)^n$, allowing

selection of either no correction ($n = 0$) for non-unity ϕ/θ or any correction the program user chooses. Thus, the program computes Stanton number from

$$C_h = \frac{\frac{C_f(R_\phi)}{2}\left(\frac{\phi}{\theta}\right)^n}{1 - 5\left(\frac{C_f(R_\phi)}{2}\right)^{1/2}\left[1 - Pr + \ln\left(\frac{6}{5Pr+1}\right)\right]} \tag{47}$$

Since $C_f(R_\phi)$ varies approximately with the $-1/4$ power of ϕ (Blasius equation), Eq. (47) gives C_h the following approximate dependence on ϕ and θ:

$$C_h \sim \frac{1}{\phi^{1/4-n}\,\theta^n} \tag{48}$$

Since C_h must depend more on ϕ than on θ, and, in particular, must approach infinity as $\phi \to 0$, it is seen that the upper limit for n is 1/4. An estimate of the actual value of n was made in Ref. 3 where a relation was employed (Eq. 26) equivalent to

$$C_h \sim \frac{1}{\theta^{1/4}\left(\frac{\phi}{\theta}\right)^{1/7}} \tag{49}$$

which is the same as Eq. (48) for $n = 3/28 \cong 0.1$. Thus, n lies between zero and 0.25, with some basis for choosing 0.1.

G. Mach Number and Heat-Transfer Relations

1. Mach Number

Mach numbers can be supplied in tabular form to the computer or they can be internally computed, where geometry permits, from the one-dimensional nozzle relation

$$\left(\frac{r}{r^*}\right)^2 = \frac{1}{M}\left[\frac{1 + \frac{\gamma-1}{2}M^2}{\frac{\gamma+1}{2}}\right]^{\frac{\gamma+1}{2(\gamma-1)}} \quad \begin{matrix} M < 1, z < z^* \\ M = 1, z = z^* \\ M > 1, z > z^* \end{matrix} \tag{50}$$

where r^* and z^* are the throat radius and axial position, respectively.

2. Heat-Transfer Coefficient

The heat-transfer coefficient h_g is defined as

$$h_g = \frac{q_w}{T_{aw} - T_w}$$

Comparison with the definition of C_h (Eq. 17) shows that

$$h_g = c_p \rho U C_h \tag{51}$$

3. Heat Flux

From the definition of h_g the heat flux is

$$q_w = h_g (T_{aw} - T_w) \tag{52-a}$$

If the gas specific heat is significantly temperature dependent or if the gas is dissociated at the free-stream stagnation temperature, these effects can be accounted for in the heat flux calculation by employing the enthalpy, instead of temperature, driving potential (Assumption 14). Thus

$$q_w = h_g\left(\frac{i_r - i_w}{c_p}\right) = \rho U C_h (i_r - i_w) \tag{52-b}$$

where i_r and i_w are the enthalpies of the gas at the adiabatic wall temperature and actual wall temperature, respectively. A convenient approximate method for computing enthalpy potential is presented in Ref. 24.

4. Cumulative Heat Transfer

The total amount of heat transferred to the wall up to the ith z-station is obtained by summing the product of q_w and the increment of wall area, dA_w, employing the mean values of q_w, wall radius, and wall slope for each interval. Thus,

$$\sum_{j=1}^{i} q_{w_j} dA_{w_j} = 2\pi \sum_{j=1}^{i} \frac{\Delta z}{2}\left\{q_{w_j} r_j \left[1 + \left(\frac{dr}{dz}\right)_j^2\right]^{1/2} + q_{w_{j-1}} r_{j-1}\left[1 + \left(\frac{dr}{dz}\right)_{j-1}^2\right]^{1/2}\right\} \tag{53}$$

H. Velocity, Temperature, and Displacement Thicknesses

The remaining boundary-layer thicknesses δ, Δ, and δ^* will next be expressed as functions of θ and ϕ through the boundary-layer shape parameters θ/δ, Δ/δ, and δ^*/θ. The integral momentum equation (Eq. 25) and integral energy equation (Eq. 30) can then be handled as two equations in the two unknowns θ and ϕ, and the remaining thicknesses can be calculated from the shape parameters.

To accomplish this it is necessary to assume distributions of velocity and temperature in the boundary layer. In accordance with Assumption 15, the distributions adopted are

$$\frac{\bar{u}}{U} = \left(\frac{y}{\delta}\right)^{1/7} \qquad y \leq \delta \tag{54}$$

$$\frac{\bar{u}}{U} = 1 \qquad y > \delta$$

and

$$\frac{\bar{t}_0 - T_w}{T_0 - T_w} = \left(\frac{y}{\Delta}\right)^{1/7} \qquad y \leq \Delta$$

$$\frac{\bar{t}_0 - T_w}{T_0 - T_w} = 1 \qquad y > \Delta \tag{55}$$

In evaluating δ, Δ, and δ^*, two cases must be considered: Case I in which the velocity thickness is less than or equal to the temperature thickness, $\delta \leq \Delta$, and Case II in which the velocity thickness is greater than the temperature thickness, $\delta > \Delta$.

1. Case I, $\delta \leq \Delta$

For the present purpose, the integral expressions for δ^*, θ, and ϕ (Eqs. 9, 12, and 15, respectively) are employed. To evaluate these integrals, the integrands must be expressed as functions of y. The ratios $\bar{u}/U$ and $(\bar{t}_0 - T_w)/(T_0 - T_w)$ are already functions of y through Eqs. (54) and (55). An expression for $\bar{\rho}/\rho$ is needed as well, and this can be obtained from the temperature distribution (Eq. 55) and the perfect gas law.

Rearranging Eq. (55) gives the stagnation temperature distribution

$$\frac{\bar{t}_0}{T_0} = \left(1 - \frac{T_w}{T_0}\right)\left(\frac{y}{\Delta}\right)^{1/7} + \frac{T_w}{T_0} \qquad y \leq \Delta$$

$$\frac{\bar{t}_0}{T_0} = 1 \qquad y > \Delta \tag{56}$$

The ratio of stagnation to static temperature in the free stream is

$$\frac{T_0}{T} = 1 + \frac{\gamma - 1}{2} M^2 \tag{57}$$

and in the boundary layer is

$$\frac{\bar{t}_0}{t} = 1 + \frac{\gamma - 1}{2}\left(\frac{\bar{u}}{\bar{c}}\right)^2 \tag{58}$$

where $\bar{t}$ is the time-mean static temperature and $\bar{c}$ is the local time-mean sonic velocity in the boundary layer. Equation (58) can be written

$$\frac{\bar{t}_0}{t} = 1 + \frac{\gamma - 1}{2}\left(\frac{\bar{u}}{U} \cdot \frac{U}{c'} \cdot \frac{c'}{\bar{c}}\right)^2 \tag{59}$$

where c' is the free-stream sonic velocity. Since U/c' is the free-stream Mach number and the sonic velocity is proportional to the square root of the gas temperature, Eq. (59) can be written

$$\frac{\bar{t}_0}{\bar{t}} = 1 + \frac{\gamma - 1}{2}\left[\frac{\bar{u}}{U} M \left(\frac{T}{\bar{t}}\right)^{1/2}\right]^2 \tag{60}$$

Rearranging Eq. (60), the static temperature distribution in the boundary layer is

$$\frac{\bar{t}}{T} = \frac{\bar{t}_0}{T_0}\left(\frac{T_0}{T}\right) - \frac{\gamma - 1}{2} M^2 \left(\frac{\bar{u}}{U}\right)^2 \tag{61}$$

Substituting Eq. (56) into Eq. (61) and rearranging yields

$$\frac{\bar{t}}{T} = \frac{T_w}{T}\left[1 + \left(\frac{T_0}{T_w} - 1\right)\left(\frac{y}{\delta}\right)^{1/7}\left(\frac{\delta}{\Delta}\right)^{1/7} - \frac{\gamma - 1}{2} M^2 \left(\frac{T}{T_w}\right)\left(\frac{\bar{u}}{U}\right)^2\right] \qquad y \leq \Delta$$

$$\frac{\bar{t}}{T} = 1 \qquad y > \Delta \tag{62}$$

In the latter equation, use is made of Eq. (57) and the fact that $\bar{u} = U$ for $y > \Delta$ in Case I.

Substituting the velocity distribution from Eq. (54) and rearranging, the final static-temperature distribution for Case I is

$$\frac{\bar{t}}{T} = a\left(1 + \frac{b}{\zeta} s - c s^2\right) \qquad y \leq \delta$$

$$= a\left(1 + \frac{b}{\zeta} s - c\right) \qquad \delta < y \leq \Delta$$

$$= 1 \qquad y > \Delta \tag{63}$$

where

$$s = \left(\frac{y}{\delta}\right)^{1/7} \tag{64}$$

$$\zeta = \left(\frac{\Delta}{\delta}\right)^{1/7} \tag{65}$$

$$a = \frac{T_w}{T} \tag{66}$$

$$b = \frac{T_0}{T_w} - 1 \tag{67}$$

and

$$c = \left(\frac{\gamma - 1}{2} M^2\right)\left(\frac{T}{T_w}\right) \tag{68}$$

Employing Assumption 6 (constant pressure across the boundary layer), the density distribution is

$$\frac{\bar{\rho}}{\rho} = \frac{T}{\bar{t}} \tag{69}$$

Substituting the temperature distribution from Eq. (63), the density distribution for Case I is

$$\begin{aligned} \frac{\bar{\rho}}{\rho} &= \frac{1}{a\left(1 + \frac{b}{\zeta} s - c s^2\right)} && y \leq \delta \\ &= \frac{1}{a\left(1 + \frac{b}{\zeta} s - c\right)} && \delta < y \leq \Delta \\ &= 1 && y > \Delta \end{aligned} \tag{70}$$

The boundary-layer thickness integrals can now be evaluated. By substituting $\bar{u}/U$ from Eq. (54) and $\bar{\rho}/\rho$ from Eq. (70) into the integral expression for the momentum thickness (Eq. 12), and noting that the integrand is zero for $y > \delta$, an expression is obtained for θ as a function of δ:

$$\theta = \int_0^\delta \frac{s(1 - s)}{a\left(1 + \frac{b}{\zeta} s - c s^2\right)} dy \tag{71}$$

Noting from Eq. (64) that $dy = 7\delta s^6\, ds$, the final expression for the momentum thickness is

$$\frac{\theta}{\delta} = \frac{7}{a} I_1 \tag{72}$$

where

$$I_1 = \int_0^1 \frac{s^7 (1 - s)}{1 + \frac{b}{\zeta} s - c s^2} ds \tag{73}$$

Substituting $\bar{u}/U$ from Eq. (54) and $\bar{\rho}/\rho$ from Eq. (70) into the integral expression for the displacement thickness (Eq. 9), and noting that the integrand is zero for $y > \Delta$, an expression is obtained for δ^* as a function of δ and Δ:

$$\delta^* = \int_0^\Delta dy - \left[\int_0^\delta \frac{s}{a\left(1 + \frac{b}{\zeta} s - c s^2\right)} dy + \int_\delta^\Delta \frac{1}{a\left(1 + \frac{b}{\zeta} s - c\right)} dy\right] \tag{74}$$

Substituting $dy = 7\delta s^6\, ds$, the final expression for the displacement thickness is

$$\frac{\delta^*}{\delta} = \zeta^7 - \frac{7}{a}(I_2 + I_3) \tag{75}$$

where

$$I_2 = \int_0^1 \frac{s^7}{1 + \frac{b}{\zeta} s - c s^2} ds \tag{76}$$

and

$$I_3 = \int_1^\zeta \frac{s^6}{1 + \frac{b}{\zeta} s - c} ds \tag{77}$$

Substituting $\bar{u}/U$ from Eq. (54), $(\bar{t}_0 - T_w)/(T_0 - T_w)$ from Eq. (55), and $\bar{\rho}/\rho$ from Eq. (70) into the integral expression for the energy thickness (Eq. 15), and noting that the integrand is zero for $y > \Delta$, an expression is obtained for ϕ as a function of δ and Δ:

$$\phi = \int_0^\delta \frac{s\left(1 - \frac{s}{\zeta}\right)}{a\left(1 + \frac{b}{\zeta} s - c s^2\right)} dy + \int_\delta^\Delta \frac{1 - \frac{s}{\zeta}}{a\left(1 + \frac{b}{\zeta} s - c\right)} dy \tag{78}$$

Defining $w = s/\zeta$ and substituting $dy = 7\delta s^6\, ds$, the final expression for the energy thickness is

$$\frac{\phi}{\delta} = \frac{7\zeta^7}{a}(\zeta I_2' + I_3') \tag{79}$$

where

$$I_2' = \int_0^{1/\zeta} \frac{w^7 (1 - w)}{1 + bw - c\zeta^2 w^2} dw \tag{80}$$

and

$$I_3' = \int_{1/\zeta}^1 \frac{w^6 (1 - w)}{1 + bw - c} dw \tag{81}$$

Dividing Eq. (75) by Eq. (72) yields the expression for δ^*/θ required in the integral momentum equation.

$$\frac{\delta^*}{\theta} = \frac{\frac{a\zeta^7}{7} - I_2 - I_3}{I_1} \tag{82}$$

Dividing Eq. (79) by Eq. (72) and rearranging yields ζ as a function of ϕ/θ.

$$\zeta = \left[\frac{\phi I_1}{\theta\left(I_2' + \frac{I_3'}{\zeta}\right)}\right]^{1/6} \tag{83}$$

2. Case II, $\delta > \Delta$

Following the same procedure as in the derivation of Eq. (70), the density distribution for Case II is

$$\begin{aligned} \frac{\tilde{\rho}}{\rho} &= \frac{1}{a\left(1 + \frac{b}{\zeta}s - cs^2\right)} && y \leq \Delta \\ &= \frac{1}{a(1 + b - cs^2)} && \Delta < y \leq \delta \\ &= 1 && y > \delta \end{aligned} \tag{84}$$

The momentum thickness is given by

$$\frac{\theta}{\delta} = \frac{7}{a}(I_4 + I_5) \tag{85}$$

where

$$I_4 = \int_0^{\zeta} \frac{s^7(1-s)}{1 + \frac{b}{\zeta}s - cs^2}\,ds \tag{86}$$

and

$$I_5 = \int_{\zeta}^{1} \frac{s^7(1-s)}{1 + b - cs^2}\,ds \tag{87}$$

The displacement thickness is given by

$$\frac{\delta^*}{\delta} = 1 - \frac{7}{a}(I_6 + I_7) \tag{88}$$

where

$$I_6 = \int_0^{\zeta} \frac{s^7}{1 + \frac{b}{\zeta}s - cs^2}\,ds \tag{89}$$

and

$$I_7 = \int_{\zeta}^{1} \frac{s^7}{1 + b - cs^2}\,ds \tag{90}$$

The energy thickness is given by

$$\frac{\phi}{\delta} = \frac{7\zeta^8}{a} I_1' \tag{91}$$

where

$$I_1' = \int_0^1 \frac{w^7(1-w)}{1 + bw - c\zeta^2 w^2}\,dw \tag{92}$$

δ^*/θ for Case II is

$$\frac{\delta^*}{\theta} = \frac{\frac{a}{7} - I_6 - I_7}{I_4 + I_5} \tag{93}$$

ζ for Case II is

$$\zeta = \left[\frac{\phi(I_4 + I_5)}{\theta I_1'}\right]^{1/6} \tag{94}$$

III. UTILIZATION OF THE PROGRAM

A. Preparation of Inputs

Figure 5 presents the forms employed for presenting the input data for card punching. The entries shown are for a sample case discussed later. Form I is for program instructions and identification. Form II is for nozzle geometry, wall temperature, Mach number, and enthalpy potential. Form III is for free-stream properties, initial conditions, and miscellaneous constants.

FORM I

Instructions and identification

7 fixed integers per card with a field width of 10

Item	Quantity or Instruction	Code	Value
1	Month	MO	10
2	Day	MDAY	9
3	Year	MYR	62
4	Case Number	NNBR	1
5	This is the last case = 1 This is not the last case = 2	NCASE	1
6	Print answers at stations specified by Item 15, Form III = 1 Print answers at stations given in Form II = 2	NPRT	2
7	Number of stations in Form II	N	31
8	Mach Numbers are to be computed = 1 Mach Numbers are given in Form II = 2	MTAB	1
9	Evaluate C_f and C_f ($R\phi$) at free-stream temperature = 1 Evaluate C_f and C_f ($R\phi$) at film temperature = 2	MPRO	2
10	Use temperature potential = 1 Use enthalpy potential = 2	MPOT	1
11	Print intermediate quantities = 1 Print final quantities only = 2	MNPR	2
12	Number of iterations allowed for convergence of ζ and M	NO	30
13	Number of intervals to use in Gaussian integration	MM	5

Fig. 5. The input forms employed with the computer program, showing entries for the sample case

FORM II

Contour, Wall Temperature, Mach Number, and Enthalpy Potential

7 floating or fixed point numbers per card with a field width of 10

Z	R	TW	AMOK	EPOT
Axial Distance, z in.	Radius, r in.	Wall Temperature, T_w °R	Mach Number M	Enthalpy Potential $\frac{(i_r - i_w)/c_p}{°R}$
0.0	2.500	1125.0		
0.2	2.486	1125.0		
0.4	2.443	1125.0		
0.6	2.367	1125.0		
0.8	2.266	1125.0		
1.0	2.150	1125.0		
1.2	2.035	1125.0		
1.4	1.919	1125.0		
1.6	1.803	1125.0		
1.8	1.688	1125.0		
2.0	1.572	1125.0		
2.2	1.456	1125.0		
2.4	1.341	1125.0		
2.6	1.225	1125.0		
2.8	1.104	1125.0		
3.0	1.010	1125.0		
3.2	0.945	1125.0		
3.4	0.904	1125.0		
3.6	0.886	1125.0		
3.66	0.885	1125.0		
3.7	0.886	1125.0		
3.8	0.891	1125.0		
4.0	0.917	1125.0		
4.2	0.965	1125.0		
4.5	1.045	1125.0		
5.0	1.180	1125.0		
5.5	1.314	1125.0		
6.0	1.448	1125.0		
6.5	1.582	1125.0		
7.0	1.716	1125.0		
7.5	1.850	1125.0		

Fig. 5. The input forms employed with the computer program, showing entries for the sample case (cont'd)

FORM III

Constants

7 floating or fixed point numbers per card with a field width of 10

Item	Symbol	Quantity	Code	Value
1	Pr	Prandtl number of gas	PR	0.83
2	c_p	Stagnation specific heat of gas, Btu/lbm°R	CP	0.567
3	γ	Stagnation specific heat ratio of gas	G	1.2
4	μ_0	Stagnation viscosity of gas, lbf·sec/ft^2	AMU	1.3 E-6
5	m	Temperature dependence of viscosity	AMEX	0.65
6	p_0	Free-stream stagnation pressure, psia	PO	300.0
7	T_0	Free-stream stagnation temperature, °R	TO	4500.0
8	r*	Radius at throat, in.	RST	0.885
9	z*	Axial distance to throat, in.	ZST	3.66
10	θ_0	Initial value of momentum thickness, in.	TZERO	0.022
11	ζ_0	Initial value of ζ	ZETA	1.01
12	-	Convergence criterion for ζ and M	RITE	0.0001
13	Δz	Length of axial increment for numerical solution of differential equations, in.	HINP	0.01
14	n	Boundary-layer interaction exponent	ANEX	0.1
15	-	Printout interval, in.	AINCR	—

Fig. 5. The input forms employed with the computer program, showing entries for the sample case (cont'd)

1. Form I

Instructions and identification data are written in Form I as follows:

Items 1–3 Write numbers of no more than two digits in the value column. These will appear as the first line of output MO = xx, DAY = xx, YEAR = xx.

Item 4 Write the case number (5 digits maximum). This will also appear at the beginning of the output.

Item 5 If several cases are to be computed, write "2" in the value column of all but the last case, for which write "1."

Item 6 To print answers at equal increments specified by Item 15, Form III, write "1" in the value column. To print answers at the z-stations used in Form II, write "2."

Item 7 Write the number of z-stations employed in Form II.

Item 8 To compute free-stream Mach numbers from the isentropic, one-dimensional relation (Eq. 50), write "1" in the value column. If Mach numbers are supplied in Form II, write "2."

Item 9 To evaluate C_f and $C_f(R_\phi)$ at the free-stream temperature (Eq. 31-a), write "1." To evaluate C_f and $C_f(R_\phi)$ at the "film" temperature (Eq. 31-b), write "2."

Item 10 To compute heat flux from temperature potential (Eq. 52-a), write "1" (no entries are required in the EPOT column of Form II in this case). To compute heat flux from enthalpy potential (Eq. 52-b), write "2" (entries are required in both the TW and EPOT column of Form II in this case).

Item 11 To print out the boundary-layer thicknesses, skin-friction coefficient, heat-transfer coefficient, heat flux, and cumulative heat transfer, write "2" in the value column. To print, in addition, the intermediate quantities discussed later, write "1" in the value column.

Item 12 Write the number of iterations to be allowed in converging on ζ. It has been found that 30 are sufficient when ζ is to be converged to 0.0001 (the latter specified in Item 12, Form III). The same number of iterations is allowed for converging on internally-computed Mach number.

Item 13 Write the number of intervals desired in the Gaussian integration of I_1 through I_3'. It has been found that 5 are sufficient to give a reasonable balance between accuracy and computing time.

Numbers from Form I are punched 7 fixed integers per card, right justified in a field of 10.

2. Form II

The nozzle contour, wall temperatures, Mach numbers, and enthalpy potentials (the latter two optional) are entered in Form II as follows:

In the "Z" column, tabulate axial distance z, in inches, from the initial station where boundary-layer thicknesses are specified in Form III. The values of z must be positive and increasing throughout.

In the "R" column, tabulate the corresponding values of the radius r, in inches, from the axis of symmetry to the wall. If Mach numbers are to be internally computed, the throat coordinates must appear in Form II, and the r value entered immediately before the throat r must not equal the throat r.

In the "TW" column, tabulate the wall temperatures T_w in °R.

In the "AMOK" column, tabulate free-stream Mach numbers M, if these are not to be computed internally.

In the "EPOT" column, tabulate enthalpy potentials, if used, in °R.

The program treats the nozzle as a series of parabolic segments between the tabulated values of z and r, with parabolic variations of T_w, M, and enthalpy potential between tabulated values. The number and spacing of z-stations should be such as to permit these second-order curve fits to give a smooth approximation to the actual nozzle contour, and to the wall temperature, Mach number, and enthalpy potential variations. The computing time is independent of the number of tabulated z-stations; hence, the nozzle can be closely defined in Form II without penalty. A minimum of three z-stations must be entered, and the maximum number for which storage is provided is 500.

3. Form III

Gas properties and other constants are tabulated in Form III as follows:

Item 1 Write the value of the Prandtl number.

Item 2 Write the value of the stagnation specific heat, c_p, in Btu/lbm °R.

Item 3 Write the value of the stagnation specific heat ratio γ.

Item 4 Write the value of the stagnation viscosity, μ_0, in lbf • sec/ft^2.

Item 5 Write the exponent, m, of the temperature dependence of viscosity used in Eq. (32).

Item 6 Write the stagnation pressure, p_0, in psia.

Item 7 Write the value of the stagnation temperature, T_0, in °R.

Item 8 Write the value of the throat radius, r^*, in inches. This is used only if Mach numbers are to be internally computed.

Item 9 Write the value of the axial distance to the throat, z^*, in inches. This is used only if Mach numbers are to be internally computed.

Item 10 Write the initial value of the momentum thickness, θ_0, in inches. If the problem is to compute the growth of the boundary layer from zero thickness, then θ_0 should be a small value such as 0.001 in. Zero cannot be used since an infinite C_f would result.

Item 11 Write the initial value of ζ, namely $\zeta_0 = (\Delta_0/\delta_0)^{1/7}$. A value of 1.0 will give a smooth start to the solution when the boundary layer is assumed to grow from zero (θ_0 small). ζ_0 must not be zero and should be large enough to make ϕ_0 not less than about 10^{-4} in.

Item 12 Write the desired difference between the last two iterations of ζ. A value of 0.0001 gives sufficient accuracy for most purposes, but some experimentation may be desirable to find the best compromise between accuracy and computing time for a particular problem. The same convergence criterion is used for internally computed Mach number.

Item 13 Write the desired increment, in inches, for the numerical solution of the integral momentum and energy equations. To obtain three-figure accuracy it is necessary to make this increment about 1/100 of r^*. Some experimentation will be necessary to find the increment which gives the best compromise between accuracy and computing time for a particular problem. The IBM 7090 computer will solve about 300 increments per minute, for MM = 5 and RITE = 0.0001.

Item 14 Write the value of the boundary-layer interaction exponent n for computing Stanton number (Eq. 47).

Item 15 If an equally spaced output has been chosen in Item 6, Form I, write the desired interval, in inches, between printout stations.

Numbers can be entered in Forms II and III in either fixed-point or floating-point form. The decimal point must always appear. The numbers are punched 7 per card in a field of 10 and floating-point numbers must be right justified.

B. Output Format

1. Short Output

Figure 6 shows the form in which the output is printed if the short output option is chosen (MNPR = 2). From left to right, each column gives the values of the following quantities:

Z	z-station, in.
R	Wall radius, r, in.
DELTA	Velocity boundary-layer thickness, δ, in.
CAP DELTA	Temperature boundary-layer thickness, Δ, in.
DELTA*	Displacement thickness, δ^*, in.
THETA	Momentum thickness, θ, in.
PHI	Energy thickness, ϕ, in.
HSUBG	Heat-transfer coefficient, h_g, Btu/in^{2}sec °R.
Q	Heat flux to the wall, q_w, Btu/in^{2}sec.
SUMQ	Cumulative heat transfer to the nozzle wall up to station z, Btu/sec.
CF/2	The half skin-friction coefficient, $C_f/2$.

MO=10 DAY= 9 YEAR=62
RUN 1

Z	R	DELTA	CAP DELTA	DELTA*	THETA	PHI	HSUBG	Q	SUMQ	CF/2
0.	2.500	0.189E-00	0.202E-00	0.584E-02	0.220E-01	0.237E-01	0.378E-03	0.128E 01	0.	0.258E-02
0.200	2.486	0.189E-00	0.205E-00	0.557E-02	0.221E-01	0.241E-01	0.380E-03	0.128E 01	0.402E 01	0.257E-02
0.400	2.443	0.181E-00	0.205E-00	0.450E-02	0.212E-01	0.242E-01	0.391E-03	0.132E 01	0.814E 01	0.258E-02
0.600	2.367	0.166E-00	0.202E-00	0.274E-02	0.196E-01	0.240E-01	0.413E-03	0.139E 01	0.125E 02	0.259E-02
0.800	2.266	0.147E-00	0.196E-00	0.761E-03	0.176E-01	0.236E-01	0.447E-03	0.151E 01	0.173E 02	0.260E-02
1.000	2.150	0.129E-00	0.188E-00	-0.104E-02	0.156E-01	0.230E-01	0.491E-03	0.166E 01	0.226E 02	0.262E-02
1.200	2.035	0.115E-00	0.181E-00	-0.239E-02	0.139E-01	0.223E-01	0.540E-03	0.182E 01	0.279E 02	0.262E-02
1.400	1.919	0.102E-00	0.174E-00	-0.340E-02	0.125E-01	0.216E-01	0.599E-03	0.202E 01	0.334E 02	0.261E-02
1.600	1.803	0.921E-01	0.166E-00	-0.412E-02	0.113E-01	0.209E-01	0.667E-03	0.225E 01	0.391E 02	0.259E-02
1.800	1.688	0.837E-01	0.159E-00	-0.461E-02	0.103E-01	0.201E-01	0.747E-03	0.252E 01	0.454E 02	0.256E-02
2.000	1.572	0.762E-01	0.152E-00	-0.490E-02	0.944E-02	0.193E-01	0.845E-03	0.285E 01	0.521E 02	0.252E-02
2.200	1.456	0.697E-01	0.144E-00	-0.504E-02	0.866E-02	0.183E-01	0.966E-03	0.326E 01	0.588E 02	0.248E-02
2.400	1.341	0.639E-01	0.136E-00	-0.506E-02	0.796E-02	0.174E-01	0.112E-02	0.377E 01	0.659E 02	0.243E-02
2.600	1.225	0.584E-01	0.128E-00	-0.498E-02	0.729E-02	0.164E-01	0.131E-02	0.441E 01	0.735E 02	0.237E-02
2.800	1.104	0.529E-01	0.119E-00	-0.481E-02	0.661E-02	0.152E-01	0.157E-02	0.528E 01	0.817E 02	0.230E-02
3.000	1.010	0.493E-01	0.112E-00	-0.463E-02	0.615E-02	0.144E-01	0.183E-02	0.615E 01	0.905E 02	0.223E-02
3.200	0.945	0.474E-01	0.108E-00	-0.448E-02	0.591E-02	0.139E-01	0.205E-02	0.686E 01	0.989E 02	0.217E-02
3.400	0.904	0.469E-01	0.107E-00	-0.440E-02	0.582E-02	0.137E-01	0.219E-02	0.734E 01	0.107E 03	0.212E-02
3.600	0.886	0.477E-01	0.108E-00	-0.439E-02	0.589E-02	0.138E-01	0.225E-02	0.750E 01	0.116E 03	0.208E-02
3.660	0.885	0.481E-01	0.109E-00	-0.442E-02	0.592E-02	0.139E-01	0.225E-02	0.749E 01	0.119E 03	0.208E-02
3.700	0.886	0.484E-01	0.110E-00	-0.445E-02	0.595E-02	0.140E-01	0.224E-02	0.744E 01	0.121E 03	0.207E-02
3.800	0.891	0.497E-01	0.112E-00	-0.449E-02	0.609E-02	0.143E-01	0.220E-02	0.730E 01	0.125E 03	0.206E-02
4.000	0.917	0.533E-01	0.119E-00	-0.464E-02	0.647E-02	0.151E-01	0.206E-02	0.680E 01	0.133E 03	0.204E-02
4.200	0.965	0.584E-01	0.129E-00	-0.488E-02	0.701E-02	0.163E-01	0.185E-02	0.607E 01	0.141E 03	0.202E-02
4.500	1.045	0.673E-01	0.146E-00	-0.515E-02	0.797E-02	0.183E-01	0.156E-02	0.510E 01	0.152E 03	0.201E-02
5.000	1.180	0.835E-01	0.176E-00	-0.541E-02	0.969E-02	0.217E-01	0.121E-02	0.394E 01	0.168E 03	0.199E-02
5.500	1.314	0.101E-00	0.207E-00	-0.547E-02	0.115E-01	0.252E-01	0.974E-03	0.313E 01	0.182E 03	0.197E-02
6.000	1.448	0.119E-00	0.239E-00	-0.536E-02	0.134E-01	0.288E-01	0.798E-03	0.256E 01	0.195E 03	0.196E-02
6.500	1.582	0.138E-00	0.272E-00	-0.511E-02	0.153E-01	0.324E-01	0.666E-03	0.212E 01	0.207E 03	0.195E-02
7.000	1.716	0.158E-00	0.306E-00	-0.471E-02	0.173E-01	0.361E-01	0.564E-03	0.179E 01	0.218E 03	0.195E-02
7.500	1.850	0.178E-00	0.340E-00	-0.412E-02	0.193E-01	0.399E-01	0.485E-03	0.153E 01	0.228E 03	0.194E-02

Fig. 6. Short output for sample case

2. Long Output

Figure 7 shows the form in which the output is printed if the long output option is chosen (MNPR = 1). Each block of numbers refers to the z-station printed at the upper left-hand corner of the block. The first line of output is the same as for the short output format. The second line gives, from left to right, T = T, TAW = T_{aw}, MACH = M, RHO* MU = ρU, ZETA = ζ, CHA = C_h, DMDZ = dM/dz, DRDZ = dr/dz, DADZ = dT_w/dz, and R(PHI) = R_ϕ. The third line gives the values of the integrals I_1, I_2, I_3, I_4, I_5, I_6, I_7, I'_1, I'_2, and I'_3. If $\delta \leq \Delta$ only I_1, I_2, I_3, I'_2, and I'_3 will be valid; if $\delta > \Delta$ only I_4, I_5, I_6, I_7, and I'_1 will be valid.

The early z-stations are repeated when the differential equations are iterated more than once, in which case the last output block for that station is the valid one. The quantities printed are the local ones at the current z-station except for (1) dM/dz, dr/dz, and dT_w/dz which are the slopes of M, r, and T_w between the current and previous z-station, and (2) δ, Δ, δ^*, and SUMQ which are updated only at short-output stations.

C. Sample Computation

The sample case entered in Forms I, II, and III of Fig. 5 is for the small rocket nozzle used as an example in Ref. 3. Figure 8 shows the contour of this nozzle. In Form I are entered the date and case number, last-case code, number of stations in Form II, and instructions to print output at the Form II stations, to compute Mach numbers, evaluate C_f at film temperature as done in Ref. 3, use temperature potential for heat transfer, use the short output, allow 30 iterations for convergence of ζ and M, and use 5 intervals in the Gaussian integrations.

In Form II are entered z and r coordinates and the assumed wall temperature of 1125°R. The 31 stations employed are illustrative of an adequate tabular representation of a nozzle of low expansion ratio; supplying entries for every 0.1 in. plus inflection points and throat (80 z-stations) changed none of the output by more than 0.7 percent.

In Form III are entered the gas properties, the throat coordinates, the initial values of θ and ζ (0.022 in. and 1.01, respectively, corresponding to growth of the velocity and temperature boundary layers from the values assumed in Case 2a, Fig. 3, Ref. 3), the specification of 0.0001 convergence for ζ, an increment of 0.01 in. for the differential equation solution (requiring 750 steps for the solution and 2.5 min computing time), and interaction exponent of 0.1 (approximating the C_h relation of Ref. 3, see Eq. 49).

The short output for this sample case is reproduced in Fig. 6 and the beginning and end of the long output in

```
                                        MO=10    DAY= 9    YEAR=62
                                        RUN     1

 Z         R        DELTA     CAP DELTA     DELTA*      THETA       PHI        HSUBG       Q          SUMQ        CF/2
0.         2.500    0.189E-00  0.202E-00   0.584E-02   0.220E-01  0.237E-01  0.378E-03  0.128E 01  0.          0.258E-02

 Z         R        DELTA     CAP DELTA     DELTA*      THETA       PHI        HSUBG       Q          SUMQ        CF/2
0.010      2.500    0.189E-00  0.202E-00   0.584E-02   0.220E-01  0.237E-01  0.378E-03  0.128E 01  0.          0.258E-02
           T          TAW        MACH       RHO*MU      ZETA        CHA        DMDZ       DRDZ       DADZ        R(PHI)
       0.450E 04  0.450E 04  0.744E-01   0.240E-00   0.101E 01  0.277E-02  0.309E-03 -0.838E-02  0.          0.163E 04
           I1         I2         I3         I4          I5         I6         I7         I1P        I2P         I3P
       0.417E-02  0.346E-01  0.259E-02   0.          0.         0.         0.         0.         0.413E-02   0.118E-04

 Z         R        DELTA     CAP DELTA     DELTA*      THETA       PHI        HSUBG       Q          SUMQ        CF/2
0.015      2.500    0.189E-00  0.202E-00   0.584E-02   0.220E-01  0.237E-01  0.378E-03  0.128E 01  0.          0.258E-02
           T          TAW        MACH       RHO*MU      ZETA        CHA        DMDZ       DRDZ       DADZ        R(PHI)
       0.450E 04  0.450E 04  0.744E-01   0.240E-00   0.101E 01  0.277E-02  0.540E-03 -0.120E-01  0.153E-02   0.164E 04
           I1         I2         I3         I4          I5         I6         I7         I1P        I2P         I3P
       0.417E-02  0.346E-01  0.259E-02   0.          0.         0.         0.         0.         0.413E-02   0.118E-04

 Z         R        DELTA     CAP DELTA     DELTA*      THETA       PHI        HSUBG       Q          SUMQ        CF/2
0.015      2.500    0.189E-00  0.202E-00   0.584E-02   0.220E-01  0.237E-01  0.378E-03  0.128E 01  0.          0.258E-02
           T          TAW        MACH       RHO*MU      ZETA        CHA        DMDZ       DRDZ       DADZ        R(PHI)
       0.450E 04  0.450E 04  0.744E-01   0.240E-00   0.101E 01  0.277E-02  0.540E-03 -0.120E-01  0.153E-02   0.164E 04
           I1         I2         I3         I4          I5         I6         I7         I1P        I2P         I3P
       0.417E-02  0.346E-01  0.259E-02   0.          0.         0.         0.         0.         0.413E-02   0.118E-04

 Z         R        DELTA     CAP DELTA     DELTA*      THETA       PHI        HSUBG       Q          SUMQ        CF/2
7.490      1.847    0.158E-00  0.306E-00  -0.471E-02   0.193E-01  0.399E-01  0.487E-03  0.154E 01  0.218E 03   0.194E-02
           T          TAW        MACH       RHO*MU      ZETA        CHA        DMDZ       DRDZ       DADZ        R(PHI)
       0.262E 04  0.429E 04  0.269E 01   0.440E-00   0.110E 01  0.195E-02  0.214E-00  0.268E-00  0.          0.716E 04
           I1         I2         I3         I4          I5         I6         I7         I1P        I2P         I3P
       0.664E-02  0.598E-01  0.589E-01   0.          0.         0.         0.         0.         0.541E-02   0.126E-02

 Z         R        DELTA     CAP DELTA     DELTA*      THETA       PHI        HSUBG       Q          SUMQ        CF/2
7.500      1.850    0.158E-00  0.306E-00  -0.471E-02   0.193E-01  0.399E-01  0.486E-03  0.154E 01  0.218E 03   0.194E-02
           T          TAW        MACH       RHO*MU      ZETA        CHA        DMDZ       DRDZ       DADZ        R(PHI)
       0.261E 04  0.429E 04  0.269E 01   0.439E-00   0.110E 01  0.195E-02  0.596E-05  0.447E-05  0.153E-02   0.716E 04
           I1         I2         I3         I4          I5         I6         I7         I1P        I2P         I3P
       0.665E-02  0.598E-01  0.589E-01   0.          0.         0.         0.         0.         0.541E-02   0.127E-02

 Z         R        DELTA     CAP DELTA     DELTA*      THETA       PHI        HSUBG       Q          SUMQ        CF/2
7.510      1.850    0.158E-00  0.306E-00  -0.471E-02   0.193E-01  0.399E-01  0.484E-03  0.153E 01  0.218E 03   0.194E-02
           T          TAW        MACH       RHO*MU      ZETA        CHA        DMDZ       DRDZ       DADZ        R(PHI)
       0.261E 04  0.429E 04  0.269E 01   0.439E-00   0.110E 01  0.195E-02  0.          0.         0.          0.714E 04
           I1         I2         I3         I4          I5         I6         I7         I1P        I2P         I3P
       0.664E-02  0.598E-01  0.587E-01   0.          0.         0.         0.         0.         0.542E-02   0.126E-02

 Z         R        DELTA     CAP DELTA     DELTA*      THETA       PHI        HSUBG       Q          SUMQ        CF/2
7.500      1.850    0.158E-00  0.306E-00  -0.471E-02   0.193E-01  0.399E-01  0.484E-03  0.153E 01  0.218E 03   0.194E-02
           T          TAW        MACH       RHO*MU      ZETA        CHA        DMDZ       DRDZ       DADZ        R(PHI)
       0.261E 04  0.429E 04  0.269E 01   0.439E-00   0.110E 01  0.195E-02  0.          0.         0.          0.714E 04
           I1         I2         I3         I4          I5         I6         I7         I1P        I2P         I3P
       0.664E-02  0.598E-01  0.588E-01   0.          0.         0.         0.         0.         0.541E-02   0.126E-02
7.500      1.850    0.178E-00  0.340E-00  -0.412E-02   0.193E-01  0.399E-01  0.485E-03  0.153E 01  0.228E 03   0.194E-02
```

Fig. 7. Portion of long output for sample case

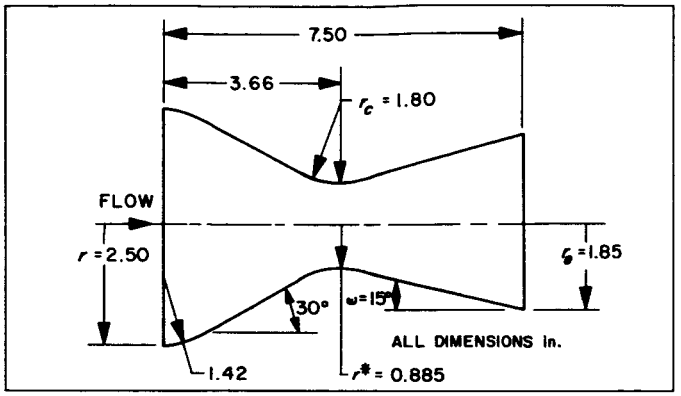

Fig. 8. Nozzle contour for sample case

Fig. 7. The computed velocity and temperature boundary-layer thicknesses are plotted in Fig. 9, as Case 2a, for comparison with Fig. 3 of Ref. 3. Included, also, are new computations of Cases 1 and 2b of Ref. 3. Comparing Fig. 9 with Fig. 3 of Ref. 3 it is seen that the only major change introduced by the present boundary-layer program (for MPRO = 2 and ANEX = 0.1) is that δ now responds to heat transfer, growing faster with large Δ (Case 2a) than with small Δ (Case 2b). This effect results from the coupling between the energy and momentum equations, which was not attempted in Ref. 3, and reflects the lesser acceleration capability of the cooler boundary layer. The other change introduced by the new program is the lower skin friction and heat transfer with the MPRO = 1 option, as discussed later.

Figure 10 presents the computed momentum and energy thicknesses for the three cases. It is seen that θ and ϕ remain about a tenth of δ and Δ, respectively, throughout the nozzle.

Figure 11 presents the displacement thickness δ^*. The negative values of δ^* throughout much of the nozzle show that, despite the velocity defect, the increased density in a severely cooled boundary layer can result in a net *increase* in the mass flux.

The heat-transfer coefficient for Cases 1, 2a, and 2b is presented in Fig. 12. It is seen that the initial momentum thickness has little effect on heat flux and that an initially thick temperature boundary layer significantly decreases heat flux as far downstream as the throat, and even beyond. Comparing Fig. 12 with Fig. 4 of Ref. 3, it is seen that the new computation (for MPRO = 2 and ANEX = 0.1) predicts about a 10% lower heat-transfer coefficient, due to the coupling of the momentum and energy equations.

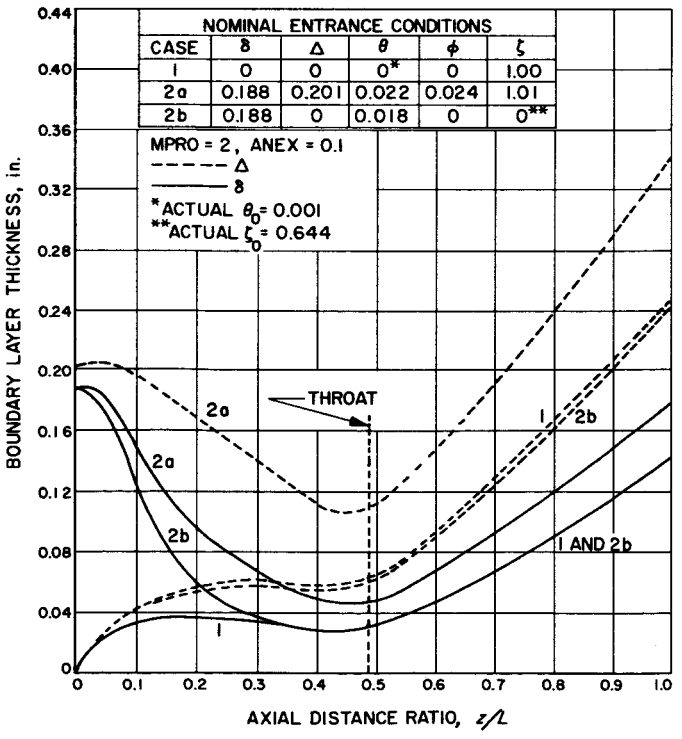

Fig. 9. Velocity and temperature thicknesses for nozzle of Fig. 8

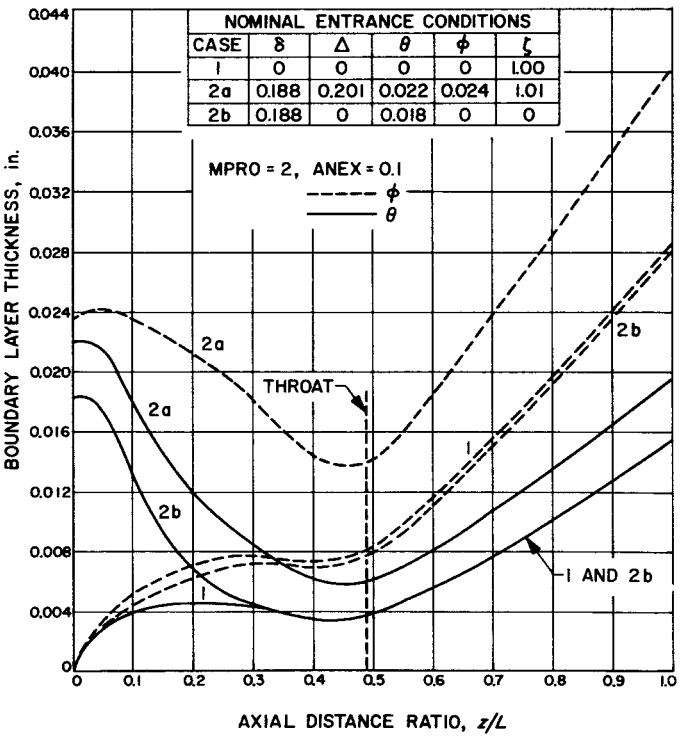

Fig. 10. Momentum and energy thicknesses for nozzle of Fig. 8

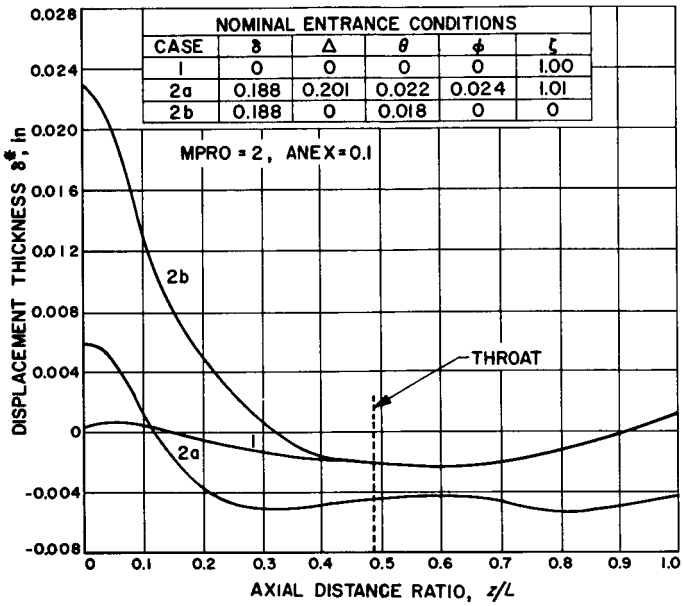

Fig. 11. Displacement thickness for nozzle of Fig. 8

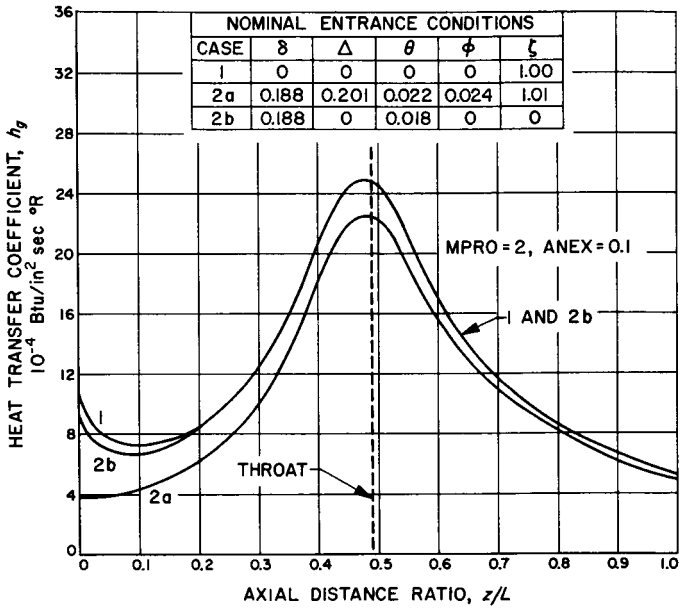

Fig. 12. Heat-transfer coefficient for nozzle of Fig. 8

IV. COMPARISON WITH EXPERIMENT

A. Heated-Air Tests

The boundary-layer program was employed to predict the heat flux in a nozzle being investigated with heated air (Ref. 25). The nozzle has a throat diameter of 1.803 in., a contraction area ratio of 7.75-to-1, an expansion area ratio of 2.68-to-1, a convergent half-angle of 30 deg, and a divergent half-angle of 15 deg. Local heat flux was measured at twenty-two stations during tests with air at $T_0 = 1500°R$ and $p_0 = 75$ to 250 psia.

For the computations, Mach numbers calculated from local wall static pressure were entered in Form II, and initial momentum thicknesses θ_0 and thickness ratios ζ_0 from nozzle-entrance probe measurements were entered in Form III. For comparison of the various program options computations were made with boundary-layer interaction exponents of both $n = 0$ and 0.1 (ANEX = 0 and 0.1), representing the probable extremes of interaction, and with C_f and C_f (R_ϕ) evaluated at both the free-stream temperature (MPRO = 1) and the film temperature (MPRO = 2). As discussed earlier, the choice of MPRO = 1 is believed to best represent the available flat-plate data, but there is insufficient data to distinguish between ANEX = 0 and 0.1.

Figure 13 compares the computed and measured heat fluxes for a stagnation pressure of 75 psia, initial momentum thickness of 0.061 in. and initial thickness ratio $\zeta_0 = 0.926$. It is seen that in the convergent section and throat the measurements agree best with the lower curves, those for MPRO = 1, and that the lowest curve, ANEX = 0, agrees with the measurements within 20% throughout the nozzle.

Figure 14 compares the computed and measured heat fluxes at a stagnation pressure of 254 psia, initial momentum thickness of 0.038 in., and thickness ratio $\zeta_0 = 0.902$. Again, except for a high heat flux in the converging sec-

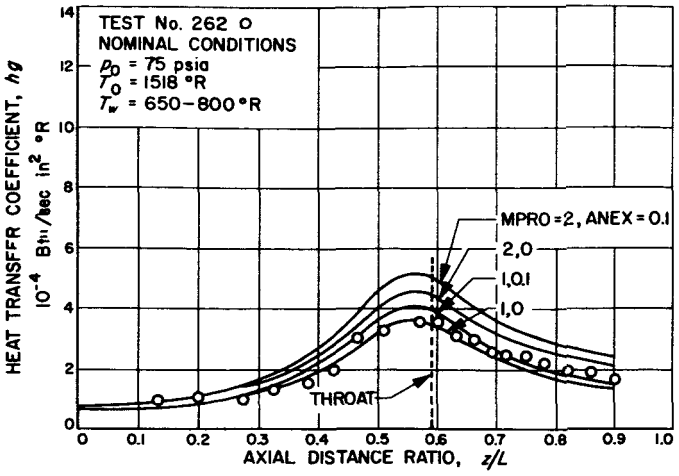

Fig. 13. Comparison of measured and computed heat-transfer coefficients for heated air at p_0 = 75 psia

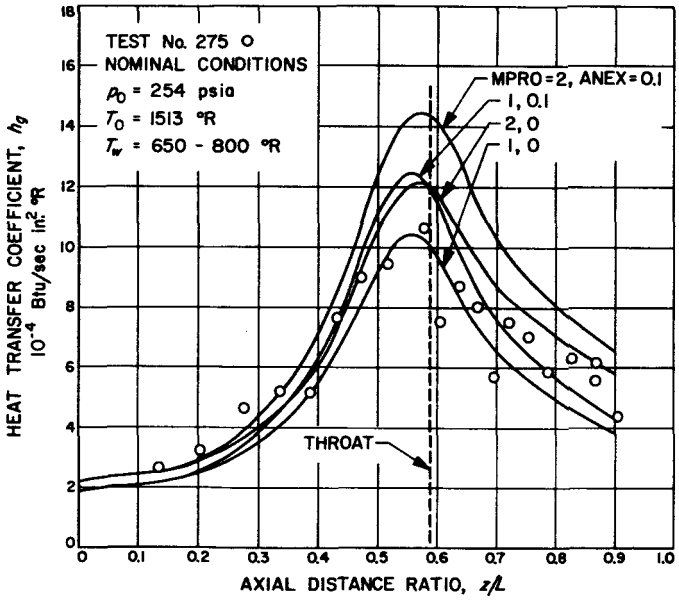

Fig. 14. Comparison of measured and computed heat-transfer coefficients for heated air at p_0 = 254 psia

tion, the predictions for MPRO = 1 agree best with the data, and the lowest curve, ANEX = 0, agrees within about 25%.

B. Rocket Motor Tests

Comparisons of computed and measured heat fluxes were made for a sectionally cooled rocket motor having a throat diameter of 2.50 in., a contraction area ratio of 4-to-1, and an expansion area ratio of 3-to-1. The motor contour is shown in the upper part of Fig. 15, and the motor is described in more detail in Ref. 24 where measured heat fluxes are presented in Fig. 6.

The computed and measured heat fluxes for tests with N_2O_4-hydrazine at a combustion pressure of p_0 = 144 psia are presented in Fig. 15. For the computations the stagnation temperature T_0 was assumed to be the adiabatic combustion temperature multiplied by the square of the ratio of measured to theoretical characteristic velocity c^*. The initial energy thickness was chosen to match the measured heat flux at the nozzle entrance, and ζ_0 was assumed to be 1.0, giving θ_0 = 0.006 in. for MPRO = 1 and θ_0 = 0.018 in. for MPRO = 2.

It is seen that the lowest prediction, MPRO = 1, ANEX = 0, falls below the data by about 25% while the highest prediction, MPRO = 2, ANEX = 0.1 (which roughly agrees with the prediction equation of Ref. 7), agrees well with the data.

Heat flux comparisons were also made for a sectionally cooled rocket motor having a throat diameter of 3.16 in.,

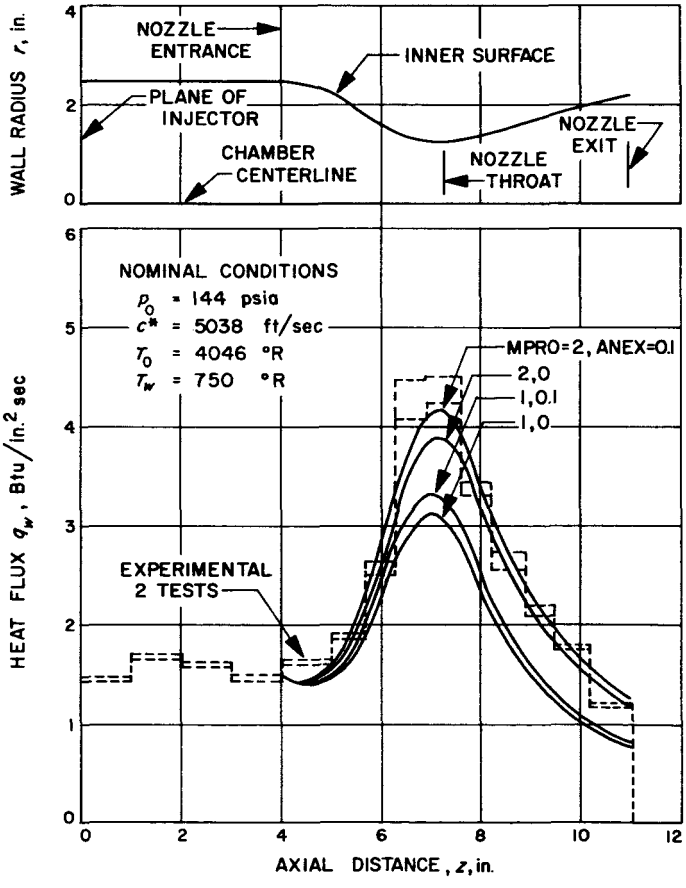

Fig. 15. Comparison of measured and computed heat fluxes for N_2O_4-hydrazine at p_0 = 144 psia

a contraction area ratio of 2.5-to-1, and an expansion area ratio of 20-to-1. The motor contour is shown in the upper part of Fig. 16, and the motor is described in more detail in Ref. 26 where measured heat fluxes are presented in Figs. 6, 7, and 8. Again, initial boundary-layer thicknesses were chosen to match the measured nozzle-entrance heat flux and ζ_0 was assumed to be 1.0, giving $\theta_0 = 0.005$ in. for MPRO = 1 and $\theta_0 = 0.015$ in. for MPRO = 2.

Figure 16 compares the computed and measured heat fluxes. It is seen that in this particular test there was a heat-flux peak immediately upstream of the throat which exceeded the predictions by factors of 1.4 to 1.9. Downstream of the throat, the predictions agree better with the measurements, and the MPRO = 1 options give the best agreement at the highest Mach numbers.

C. *Evaluation of Comparisons*

In comparing computed and measured heat fluxes it must be kept in mind that the flat-plate Stanton number correlation, Eq. (46), is only the mean of data which scatters ±15% (see Fig. 4). Thus, the heated-air nozzle tests, Figs. 13 and 14, agree with the MPRO = 1, ANEX = 0 curves within about the uncertainty of the Stanton number correlation. However, further data of this type must be obtained over a wider range of conditions to definitively test the analysis in general and the MPRO = 1, ANEX = 0 options in particular.

The simplest explanation for the discrepancy between the MPRO = 1, ANEX = 0 curves and the rocket-motor heat fluxes, Figs. 15 and 16, is that convection related to the mean free-stream flow conditions is only one of several processes affecting the net heat transfer, others being related to secondary flows dominated by injection, mixing, and combustion processes. As will be clear from a study of the data presented in Refs. 24 and 26, any prediction of heat transfer based on convection related to the mean flow conditions in a rocket motor may well be in error by as much as a factor of two because of these secondary flows.

Since rocket-motor heat fluxes are usually above, rather than below, the convective value represented by MPRO = 1 and ANEX = 0 (except at low chamber pressures, Ref. 26), the best rocket-motor predictions will usually be obtained by employing MPRO = 2 and some finite value of ANEX such as 0.1. If, indeed, rocket-motor heat flux predictions are all that are desired, and the motor geometry permits, one might as well use the simple prediction equation of Ref. 7 (which agrees closely with MPRO = 2, ANEX = 0.1) in conjunction with a safety factor adequate to accommodate the significant deviations from this equation which occur under certain conditions, as discussed in Refs. 24 and 26.

It is recommended, then, that the present program with MPRO = 1 and ANEX = 0 be employed when it is desired to compute nozzle boundary-layer growth and heat transfer corresponding to smooth, uniform, nonreacting, free-stream flow. For predicting rocket-motor heat flux, it is recommended that a large safety factor—or the MPRO = 2, ANEX = 0.1 option, or equation of Ref. 7, with a smaller safety factor—be employed.

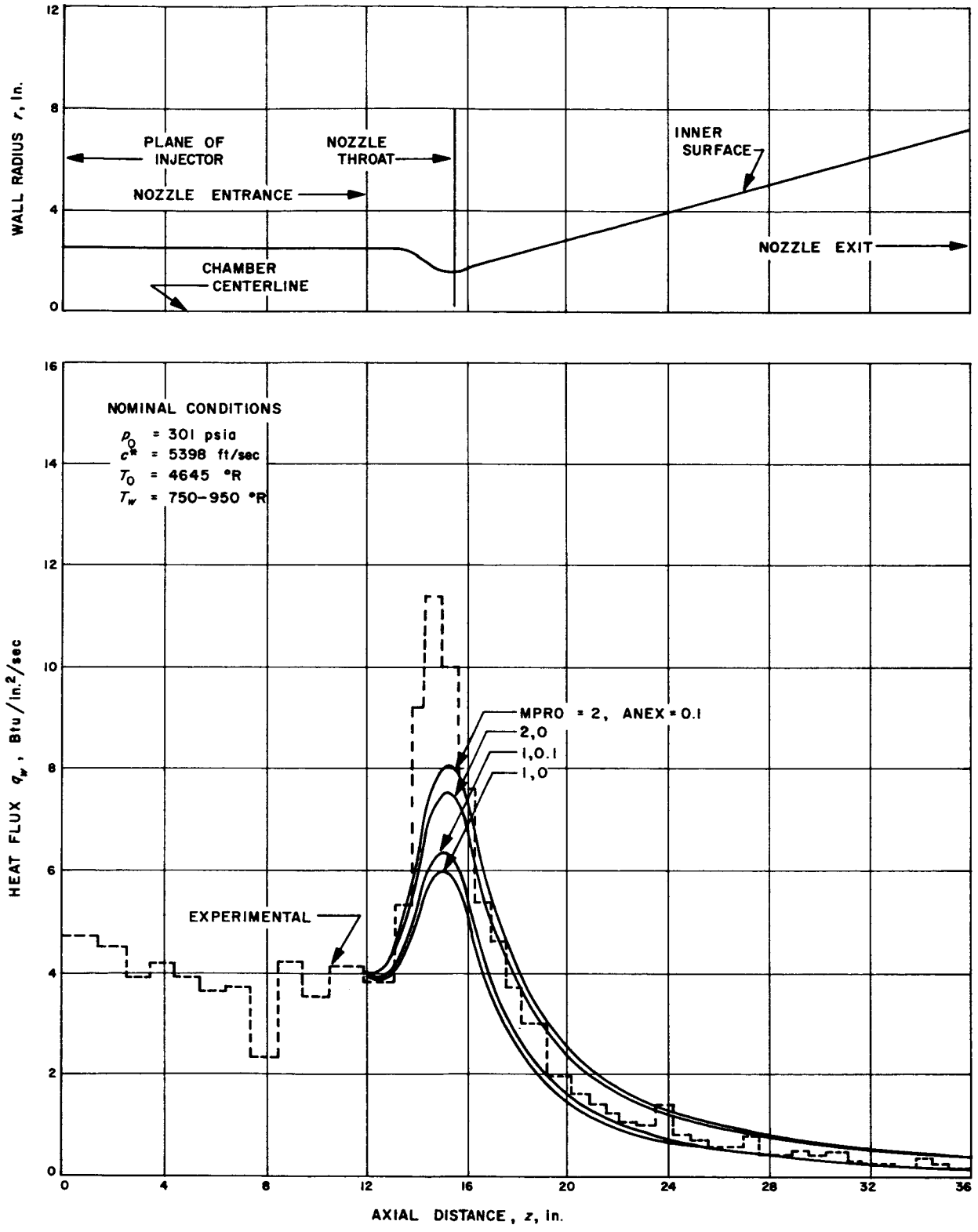

Fig. 16. Comparison of measured and computed heat fluxes for N_2O_4-hydrazine at p_0 = 301 psia

V. EFFECT OF BOUNDARY-LAYER GROWTH ON ROCKET MOTOR PERFORMANCE

A. Analysis

A secondary result of the boundary-layer program is to permit precise computation of the theoretical performance of a rocket motor with all friction and heat-transfer effects included. The relations for computing these performance corrections will be derived in this Section. The analysis, which applies generally to any axi-symmetric supersonic nozzle, will be performed with reference to the plug nozzle shown in Fig. 17.

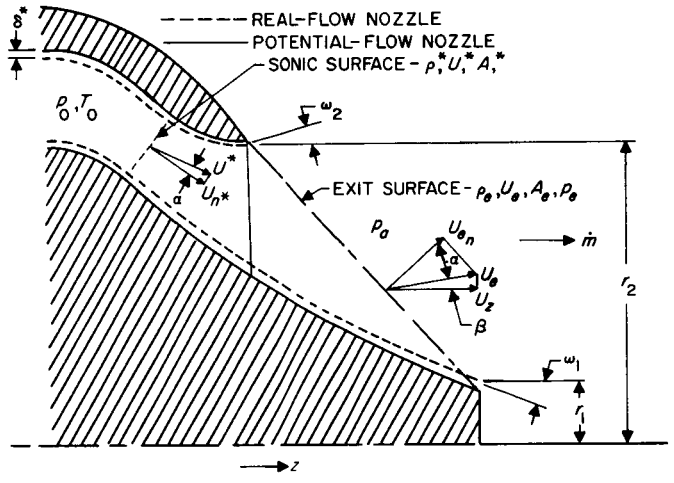

Fig. 17. Nomenclature for performance analysis

The dotted lines in Fig. 17 represent the actual, real-flow nozzle for which boundary-layer growth and heat transfer have been computed for both walls. Now, by the physical definition of δ^*, Eq. (8), the corresponding potential-flow nozzle which has the same flow rate, but has free-stream conditions extending to the walls, is obtained from the actual nozzle by moving the walls inward toward the flow by a distance δ^* at each point. The resulting potential-flow nozzle, for negative δ^*, is shown by the solid lines in Fig. 17. The following derivations, Eqs. (95) through (100), will apply to this potential-flow nozzle.

The first step is to determine the sonic and the exit surfaces of the potential-flow nozzle. The exit surface is a constant-Mach-number surface which intersects the nozzle walls along lines downstream of which the pressure acting on the walls is the ambient pressure p_a. The flow rate across the sonic surface is

$$\dot{m}_p' = \int_s \rho\, U_n\, dA \tag{95}$$

where A and U_n are, respectively, the area of, and velocity normal to, a constant-property surface, in this case the sonic surface.

The density and absolute velocity are constant along the sonic surface and they will be designated ρ^* and U^*, respectively. Eq. (95) can then be written

$$\dot{m}_p' = \rho^*\, U^*\, A_p^* \int_s \cos\alpha\, \frac{dA}{A_p^*} \tag{96}$$

where A_p^* is the area of the sonic surface of the potential-flow nozzle and α is the angle between the vector velocity and the normal to a constant-property surface, in this case the sonic surface.

Similarly, the flow rate can be written in terms of conditions along the exit surface. Thus,

$$\dot{m}_p' = \rho_e\, U_e\, A_{e_p} \int_e \cos\alpha\, \frac{dA}{A_{e_p}} \tag{97}$$

where ρ_e and U_e are the density and absolute velocity, respectively, along the exit surface and A_{e_p} is the area of the exit surface of the potential-flow nozzle.

Equating Eqs. (96) and (97) yields the ratio of the sonic flow density to the exit flow density, which is the effective expansion area ratio of both the real and potential-flow nozzles. Thus,

$$\varepsilon_{eff} = \frac{\rho^*\, U^*}{\rho_e\, U_e} = \frac{A_{e_p} \displaystyle\int_e \cos\alpha\, \frac{dA}{A_{e_p}}}{A_p^* \displaystyle\int_s \cos\alpha\, \frac{dA}{A_p^*}} \tag{98}$$

The "velocity thrust" F_{v_p} of the potential-flow nozzle is equal to the axial component of the momentum flux across the exit surface. Thus

$$F_{v_p} = \int_e \rho\, U_n\, U_z\, dA \tag{99}$$

where U_z is the axial component of the exit velocity. Denoting the angle between the vector exit velocity and the axial direction by β, Eq. (99) can be written

$$F_{v_p} = \rho_e U_e^2 A_{e_p} \int_e \cos\alpha \cos\beta \frac{dA}{A_{e_p}} \tag{100}$$

Returning, now, to the real nozzle, the difference between the velocity thrusts of the real and potential-flow nozzles is equal to the difference between the axial components of exit momentum. Hence, from the physical definition of the momentum thickness θ, Eq. (11), and from inspection of Fig. 17, the velocity thrust of the real nozzle is

$$F_{v_r} = F_{v_p} - 2\pi \rho_e U_e^2 (r_1 \theta_{e_1} \cos\omega_1 + r_2 \theta_{e_2} \cos\omega_2) \tag{101}$$

where θ_e is the exit momentum thickness and ω is the wall divergence angle, subscripts 1 and 2 referring to the inner and outer walls, respectively.

The pressure thrust of the real nozzle is equal to the pressure difference $p_e - p_a$ acting over the projected exit area $\pi(r_2^2 - r_1^2)$. Thus, employing Eq. (100), the total thrust of the real nozzle is

$$F_r = \rho_e U_e^2 A_{e_p} \times \left[\int_e \cos\alpha \cos\beta \frac{dA}{A_{e_p}} - \frac{2\pi}{A_{e_p}} (r_1 \theta_{e_1} \cos\omega_1 + r_2 \theta_{e_2} \cos\omega_2) \right] + \pi (r_2^2 - r_1^2)(p_e - p_a) \tag{102}$$

Substituting $\rho_e U_e A_{e_p}$ from Eq. (97) and recalling that $\dot{m}'_r = \dot{m}'_p$, the thrust can be written

$$F_r = \frac{\dot{m}'_r U_e}{\int_e \cos\alpha \frac{dA}{A_{e_p}}} \times \left[\int_e \cos\alpha \cos\beta \frac{dA}{A_{e_p}} - \frac{2\pi}{A_{e_p}} (r_1 \theta_{e_1} \cos\omega_1 + r_2 \theta_{e_2} \cos\omega_2) \right] + \pi (r_2^2 - r_1^2)(p_e - p_a) \tag{103}$$

The specific impulse, I_s, characteristic velocity c^*, and thrust coefficient C_F for the real nozzle are then obtained from the usual definitions:

$$I_{s_r} = \frac{F_r}{\dot{m}'_r} \tag{104}$$

$$c^*_r = \frac{p_0 A_t}{\dot{m}'_r} \tag{105}$$

$$C_{F_r} = \frac{F_r}{p_0 A_t} \tag{106}$$

where A_t is the geometric throat area–the minimum planar cross-sectional area of the nozzle.

The procedure for determining the theoretical performance of a rocket motor with friction and heat transfer effects included is, therefore, as follows:

1. Compute the boundary layer thicknesses δ^* and θ for the nozzle.
2. Locate the potential-flow nozzle contour by displacing the real nozzle contour inward toward the flow by δ^* (inward by δ^* for positive δ^* and outward by $|\delta^*|$ for negative δ^*).
3. Determine, by the method of characteristics or other means, the contours and areas of the sonic and exit surfaces and evaluate the integrals

$$\int_s \cos\alpha \, dA/A^*_p, \int_e \cos\alpha \, dA/A_{e_p}, \text{ and } \int_e \cos\alpha \cos\beta \, dA/A_{e_p}.$$

4. From Eq. (98), compute the effective expansion area ratio of the nozzle.
5. From thermochemical data for the desired stagnation conditions, determine the exit velocity U_e and exit pressure p_e corresponding to the effective expansion ratio.
6. From Eq. (96) or (97), compute the flow rate through the nozzle.
7. From Eqs. (103), (104), (105), and (106), compute the thrust, specific impulse, characteristic velocity, and thrust coefficient of the nozzle.

B. Example

As an example, the theoretical flow rate, thrust, specific impulse, characteristic velocity, and thrust coefficient will be calculated for the nozzle of Fig. 8, for an ambient pressure of 14.1 psia, and compared with the one-dimensional values.

From Fig. 6 the displacement thickness at the throat is

$$\delta^*_t = -0.00442 \text{ in.}$$

and the displacement thickness at the exit is

$$\delta^*_e = -0.00412 \text{ in.}$$

Hence, the potential-flow nozzle of equal flow rate has a throat radius of

$$r^*_p = 0.885 + 0.00442 = 0.88942 \text{ in.}$$

and, taking account of the 15-deg divergence angle, an exit radius of

$$r_{e_p} = 1.850 + 0.00412 \cos 15^\circ$$
$$= 1.85398 \text{ in.}$$

The net effect of sonic-surface curvature is a deviation of the flow rate from the one-dimensional value by a factor C_D. Thus

$$m'_p = C_D \rho^* U^* A_{t_p} \tag{107}$$

and, from Eq. (96),

$$A^*_p \int_s \cos\alpha \frac{dA}{A^*_p} = C_D A_{t_p} \tag{108}$$

Based on a variety of assumptions for the transonic flow, various values of C_D have been presented as functions of the ratio of throat radius to axial radius of curvature r^*/r_c (Refs. 27, 28, 29, 30). The values, all between 0.98 and 1.0, differ by so little that experiments are too insensitive to distinguish which is the correct approach. Here, a value from Ref. 27 has been selected for the ratio $r^*/r_c = 0.49$ of Fig. 8, the value being $C_D = 0.993$.

The throat area of the potential-flow nozzle is

$$A_{t_p} = \pi (0.88942)^2$$
$$= 2.4852 \text{ in.}^2$$

Hence, from Eq. (108),

$$A^*_p \int_s \cos\alpha \frac{dA}{A^*_p} = (0.993)(2.4852)$$
$$= 2.4678 \text{ in.}^2$$

The exit surface of a conical nozzle is spherical with the vector velocity perpendicular to the surface. Hence

$$\int_e \cos\alpha \frac{dA}{A_{e_p}} = 1$$

It can readily be verified that for the spherical exit surface

$$A_{e_p} = \frac{2\pi r^2_{e_p}}{1 + \cos 15^\circ}$$
$$= 10.9855 \text{ in.}^2$$

and

$$\int_e \cos\alpha \cos\beta \frac{dA}{A_{e_p}} = \frac{1 + \cos 15^\circ}{2}$$
$$= 0.98297$$

From Eq. (98) the effective expansion area ratio is

$$\varepsilon_{eff} = \frac{10.9855}{2.4678}$$
$$= 4.4515$$

Ordinarily, thermochemical computations would be employed at this point to determine the sonic and exit conditions. However, for simplicity, isentropic constant-property relations will be employed, using the stagnation conditions of Form III, Fig. 5. The pressure ratio is given by

$$\frac{1}{\varepsilon_{eff}} = \left(\frac{\gamma+1}{2}\right)^{\frac{1}{\gamma-1}} \left(\frac{p_e}{p_0}\right)^{\frac{1}{\gamma}} \sqrt{\frac{\gamma+1}{\gamma-1}\left[1 - \left(\frac{p_e}{p_0}\right)^{\frac{\gamma-1}{\gamma}}\right]} \tag{109}$$

For $\varepsilon_{eff} = 4.4515$ the pressure ratio is

$$\frac{p_0}{p_e} = 26.69$$

and the exit pressure is

$$p_e = \frac{300}{26.69}$$
$$= 11.24 \text{ psia}$$

The exit velocity is

$$U_e = \sqrt{2 c_p T_0 \left[1 - \left(\frac{p_e}{p_0}\right)^{\frac{\gamma-1}{\gamma}}\right]}$$
$$= 7339 \text{ ft/sec} \tag{110}$$

From Eq. (36), the sonic mass flux is

$$\rho^* U^* = 1.9184 \text{ lbm/sec in.}^2$$

From Eq. (96), the flow rate is

$$\dot{m}'_r = \dot{m}'_p = (1.9184)(2.4678)$$
$$= 4.7342 \text{ lbm/sec}$$

From Fig. 6, the exit momentum thickness is

$$\theta_e = 0.0193 \text{ in.}$$

Since there is only one wall, there is only one $r\theta_e \cos\omega$ term in Eq. (103), namely

$$r\theta_e \cos\omega = (1.850)(0.0193)\cos 15^\circ$$
$$= 0.0345$$

From Eq. (103), the thrust is

$$F_r = \frac{(4.7342)(7339)}{(1)(32.174)}\left[(0.98297) - \left(\frac{2\pi}{10.9855}\right)(0.0345)\right]$$
$$+ \pi(1.85)^2(11.24 - 14.10)$$
$$= 1009.4 \text{ lbf}$$

Noting that the geometric throat area is

$$A_{t_r} = \pi(0.885)^2 = 2.4606 \text{ in.}^2$$

then Eqs. (104), (105), and (106) give

$$I_{s_r} = \frac{1009.4}{4.7342}$$
$$= 213.2 \text{ lbf} \cdot \text{sec/lbm}$$
$$c^*_r = \frac{(300)(2.4606)(32.174)}{4.7342}$$
$$= 5017 \text{ ft/sec}$$
$$C_{F_r} = \frac{1009.4}{(300)(2.4606)}$$
$$= 1.367$$

It is of interest to compare these quantities with the simple one-dimensional values. The geometric area ratio of the nozzle is

$$\varepsilon = \left(\frac{1.85}{0.885}\right)^2$$
$$= 4.3698$$

The corresponding pressure ratio is

$$\frac{p_0}{p_e} = 26.01$$

and the exit pressure is

$$p_e = \frac{300}{26.01}$$
$$= 11.53 \text{ psia}$$

The exit velocity is

$$U_e = 7317 \text{ ft/sec}$$

The flow rate is

$$\dot{m}' = (1.9184)(\pi)(0.885)^2$$
$$= 4.7204 \text{ lbm/sec}$$

The thrust is

$$F = \frac{(4.7204)(7317)}{32.174} + \pi(1.85)^2(11.53 - 14.10)$$
$$= 1073.5 - 27.6$$
$$= 1045.9 \text{ lbf}$$

The one-dimensional values of I_s, c^*, and C_f are

$$I_s = \frac{1045.9}{4.7204}$$
$$= 221.6 \text{ lbf} \cdot \text{sec/lbm}$$
$$c^* = \frac{(300)(2.4606)(32.174)}{4.7204}$$
$$= 5031 \text{ ft/sec}$$
$$C_F = \frac{1045.9}{(300)(2.4606)}$$
$$= 1.417$$

It has been customary in the past to correct the velocity thrust term by the factor $(1 + \cos\omega)/2$, to correct for divergence, and by an empirical "discharge coefficient" often taken as 0.985. The resulting corrected one-dimensional thrust is

$$F = (1073.5)(0.98297)(0.985) - 27.6$$
$$= 1011.8 \text{ lbf}$$

The corresponding corrected values of I_s and C_F are

$$I_s = \frac{1011.8}{4.7204}$$
$$= 214.3 \text{ lbf} \cdot \text{sec/lbm}$$
$$C_F = \frac{1011.8}{(300)(2.4606)}$$
$$= 1.371$$

The exact, one-dimensional, and corrected one-dimensional results are compared in Table 2. It is seen that the corrected one-dimensional values are close to the exact values for this simple conical nozzle.

Table 2. Comparison of exact, one-dimensional, and corrected one-dimensional performance parameters

Parameter	Exact	One-dimensional	Corrected
$\dot{m}$	4.7342	4.7204	—
ε	4.4515	4.3698	—
P_0/P_e	26.69	26.01	—
P_e	11.24	11.53	—
F	1009.4	1045.9	1011.8
I_s	213.2	221.6	214.3
c^*	5017	5031	—
C_F	1.367	1.417	1.371

ACKNOWLEDGEMENTS

The authors gratefully acknowledge the contribution of Ying-Nien Yu in formulating the basic mathematical approach to the simultaneous solution of the boundary-layer equations. They are also indebted to Helmut Wolf for helpful discussions regarding available skin-friction and heat-transfer data, and to Arvel B. Witte, Edward Y. Harper, and Harold L. Gier for assistance in preparing comparisons with their carefully obtained nozzle heat-transfer data.

NOMENCLATURE

A Flow area

A_t Geometric throat area

A_w Wall area

a Parameter defined by Eq. (66)

b Parameter defined by Eq. (67)

C_D Sonic-flow coefficient

C_F Thrust coefficient

C_f Skin-friction coefficient based on R_θ

$C_f(R_\phi)$ Skin-friction coefficient based on R_ϕ.

C_{f_a} Adiabatic skin-friction coefficient

$\bar{C}_f$ Low-speed adiabatic skin-friction coefficient

C_h Stanton number

c Parameter defined by Eq. (68)

c^* Characteristic velocity

$\bar{c}$ Local mean sonic velocity in the boundary layer

c' Sonic velocity at the edge of the boundary layer

c_p Specific heat of the gas

F Thrust

F_v Velocity thrust

$\dot{H}$ Enthalpy flux of the wall flow

h_g Heat-transfer coefficient

I_s Specific impulse

$I_1 \cdots I_3'$ Integrals in the shape parameters

i_r Recovery enthalpy of the gas

i_w Enthalpy of the gas at the wall temperature

L Nozzle length

M Mach number at the edge of the boundary layer

$\dot{M}$ Momentum flux of the wall flow

m Exponent of temperature dependence of viscosity

$\dot{m}$ Wall mass flux

$\dot{m}'$ Nozzle flow rate

n Boundary-layer interaction exponent

Pr Prandtl number of the gas at stagnation conditions

p Static pressure at the edge of the boundary layer

p_a Ambient pressure

p_o Stagnation pressure of the gas

q_w Heat flux to the wall

R Adiabatic recovery factor

R_θ Reynolds number based on momentum thickness

R_ϕ Reynolds number based on energy thickness

$\bar{R}_{\bar{\theta}}$ Low-speed Reynolds number corresponding to R_θ

r Radius from nozzle axis to wall

r^* Throat radius

r_c Radius of axial curvature at the throat.

s Dummy variable in integrals.

T Static temperature at the edge of the boundary layer.

T_0 Stagnation temperature.

T_s Sublayer temperature in Coles' transformation.

T_w Wall temperature.

T_{aw} Adiabatic wall temperature.

$\bar{t}$ Local time-mean static temperature in the boundary layer.

$\bar{t}_0$ Local time-mean stagnation temperature in the boundary layer.

U Velocity at the edge of the boundary layer.

U_n Velocity component normal to constant-property surface.

U_z Axial velocity component.

$\bar{u}$ Local time-mean x-component of velocity in the boundary layer.

NOMENCLATURE (Cont'd)

w Dummy variable in integrals.

x Distance along wall.

y Distance from wall.

z Distance along axis of symmetry.

z^* Axial distance to throat.

α Angle between vector velocity and normal to constant-property surface.

β Angle between vector velocity and axial direction.

γ Specific heat ratio of the gas at stagnation conditions.

Δ Temperature thickness of the boundary layer.

δ Velocity thickness of the boundary layer.

δ^* Displacement thickness of the boundary layer.

δ' Thickness of wall flow.

ε Expansion area ratio.

ζ Shape parameter $(\Delta/\delta)^{1/7}$

θ Momentum thickness of the boundary layer.

ω Exit divergence angle.

μ Viscosity of the gas at the edge of the boundary layer.

μ_0 Viscosity of the gas at stagnation conditions.

μ_s Viscosity of the gas at T_s.

μ_{aw} Viscosity of the gas at the adiabatic wall temperature.

ρ Gas density at the edge of the boundary layer.

ρ_{aw} Gas density at the adiabatic wall temperature.

$\bar{\rho}$ Local time-mean density in the boundary layer.

τ_w Retarding wall shear stress.

ϕ Energy thickness of the boundary layer.

Subscripts

$_e$ Exit surface.

$_p$ Potential flow.

$_r$ Real flow.

REFERENCES

1. McAdams, W. H., *Heat Transmission,* Third Edition, p. 219, McGraw-Hill Book Company, Inc., New York, 1954.
2. Sibulkin, M., "Heat Transfer to an Incompressible Turbulent Boundary Layer and Estimation of Heat-Transfer Coefficients at Supersonic Nozzle Throats," *Journal of the Aeronautical Sciences,* Vol. 23 (2), pp. 162–172, February 1956.
3. Bartz, D. R., "An Approximate Solution of Compressible Turbulent Boundary-Layer Development and Convective Heat Transfer in Convergent-Divergent Nozzles," ASME Transactions, Vol. 77, (8), pp. 1235–1245, November 1955.
4. Tucker, M., "Approximate Calculation of Turbulent Boundary-Layer Development in Compressible Flow," *NACA TN 2337,* April 1951.
5. Gomf, G. E. "Supersonic Nozzle Design for Viscous Fluids," Thesis in Aeronautical Engineering, California Institute of Technology, Pasadena, California, 1949.
6. Tetervin, N., "Approximate Formulas for the Computation of Turbulent Boundary-Layer Momentum Thicknesses in Compressible Flows," *NACA Wartime Report No. L119,* March 1946.
7. Bartz, D. R., "A Simple Equation for Rapid Estimation of Rocket Nozzle Convective Heat Transfer Coefficients," *Jet Propulsion,* Vol. 27 (1), pp. 49–51, January 1957.
8. Coles, D. E., "The Turbulent Boundary Layer in a Compressible Fluid," *Report No. P-2417,* The Rand Corporation, Santa Monica, California, August 22, 1961.
9. Shapiro, A. H., *The Dynamics and Thermodynamics of Compressible Fluid Flow, Volume II,* The Ronald Press Company, New York, 1954.
10. Ludwieg, H., and W. Tillman, "Investigation of the Wall-Shearing Stress in Turbulent Boundary Layers," *NACA TM 1285,* May 1950.
11. Lobb, R. K., E. M. Winkler, and J. Persh, "Experimental Investigation of Turbulent Boundary Layers in Hypersonic Flow," *Journal of the Aeronautical Sciences,* Vol. 22, No. 1, pp. 1–10, January 1955.
12. Reynolds, W. C., W. M. Kays, and S. J. Kline, "Heat Transfer in the Turbulent Incompressible Boundary Layer with Constant Wall Temperature," *NASA Memorandum 12-1-58W,* December 1958.
13. Wolf, H., "The Experimental and Analytical Determination of the Heat Transfer Characteristics of Air and Carbon Dioxide in the Thermal Entrance Region of a Smooth Tube with Large Temperature Differences Between the Gas and the Tube Wall," Ph.D. Thesis, Purdue University, Lafayette, Indiana, March 1958.
14. Zellnik, H. E., and S. W. Churchill, "Convective Heat Transfer from High-Temperature Air Inside a Tube," *Journal of the American Institute of Chemical Engineers,* Vol. 4, No. 1, pp. 37–42, March 1958.
15. Eckert, E. R. G., "Survey on Heat Transfer at High Speeds," *WADC Technical Report 54-70,* Wright Air Development Center, April 1954.
16. Dittus, F. W., and L. M. K. Boelter, *Univ. Calif. Pub. in Eng.,* Vol. 2, p. 443, 1930.
17. Colburn, A. P., "A Method of Correlating Forced Convection Heat Transfer Data and a Comparison with Fluid Friction," *Transactions of the American Institute of Chemical Engineers,* Vol. 29, pp. 174–210, 1933.
18. Humble, L. V., W. H. Lowdermilk, and L. G. Desmon, "Measurements of Average Heat-Transfer and Friction Coefficients for Subsonic Flow of Air in Smooth Tubes at High Surface and Fluid Temperatures," *NACA Report 1020,* 1951.
19. Scherrer, R., and F. E. Gowen, "Comparison of Theoretical and Experimental Heat-Transfer on a Cooled 20° Cone with a Laminar Boundary Layer at a Mach Number of 2.02," *NACA TN 2087,* May 1950.
20. Slack, E. G., "Experimental Investigation of Heat Transfer Through Laminar and Turbulent Boundary Layers on a Cooled Flat Plate at a Mach Number of 2.4," *NACA TN 2686,* April 1952.
21. Van Driest, E. R., "The Turbulent Boundary Layer for Compressible Fluids on a Flat Plate With Heat Transfer," *North American Aviation Report AL-1914,* February 20, 1950.
22. Deissler, R. G., and A. L. Loeffler, Jr., "Turbulent Flow and Heat Transfer on a Flat Plate at High Mach Numbers with Variable Fluid Properties," *NASA TR R-17,* 1959.
23. Eckert, E. R. G., and R. M. Drake, Jr., *Heat and Mass Transfer,* McGraw-Hill Book Company, Inc., New York, 1959.

REFERENCES (Cont'd)

24. Welsh, W. E. Jr., and A. B. Witte, "A Comparison of Analytical and Experimental Local Heat Fluxes in Liquid-Propellant Rocket Thrust Chambers," Technical Report No. 32-43, Jet Propulsion Laboratory, Pasadena, February 1, 1961.

25. Massier, P. F., and H. L. Gier, "Convective Heat Transfer in Nozzles," *Research Summary No. 36-11*, pp. 80–89, Jet Propulsion Laboratory, Pasadena, November 1, 1961.

26. Witte, A. B., and E. Y. Harper, "Experimental Investigation and Empirical Correlation of Local Heat-Transfer Rates in Rocket-Engine Thrust Chambers," Technical Report No. 32-244, Jet Propulsion Laboratory, Pasadena, March 19, 1962.

27. Rao, G. V. R., "Evaluation of Conical Nozzle Thrust Coefficient," *ARS Journal*, Vol. 29 (8), p. 606, August 1959.

28. Snow, R. M., "Variational Methods in the Theory of Gas Flow Through Nozzles," Applied Physics Laboratory, Johns Hopkins University, CM 535, August 8, 1949.

29. Oswatitsch, K., and W. Rothstein, "Flow Pattern in a Converging-Diverging Nozzle," *NACA TM 1215*, 1949.

30. Kuhns, R., "Flow Separation in Overexpanded Supersonic Nozzles," *Report No. RT-124*, Consolidated Vultee Aircraft Corp., San Diego, Calif., 1952.

APPENDIX
Summary of Equations and Numerical Procedures Employed in Program

For the convenience of those employing the computer program, the equations directly utilized in the program are reproduced in this Appendix. They will be designated by the same numbers employed previously. The numerical procedures employed in the program will also be outlined.

A. Input Tables

Interpolation in the input tables of r, T_w, M, and enthalpy potential (Form II) is accomplished by subroutine INTERP, a Lagrangian interpolation routine employed in second order.

B. Auxiliary Input Quantities

1. Mach Number

If MATB = 1, Mach numbers are computed from

$$\left(\frac{r}{r^*}\right)^2 = \frac{1}{M}\left[\frac{1+\frac{\gamma-1}{2}M^2}{\frac{\gamma+1}{2}}\right]^{\frac{\gamma+1}{2(\gamma-1)}} \qquad \begin{matrix} M<1, z<z^* \\ M=1, z=z^* \\ M>1, z>z^* \end{matrix} \tag{50}$$

Equation 50 is solved iteratively by a Newton-Raphson second-order process employing the previous M as the initial guess, except for the first subsonic and supersonic Mach numbers which employ 0.5 and 1.2, respectively, as the first guess. A maximum of NO iterations are allowed for achieving a difference less than RITE between the last two iterations, failing which the computer prints "Mach could not converge." When the computer reaches z^* it sets M = 1 and switches to the supersonic branch of Eq. (50). If, due to an error in preparation of Form II or in the values of z^* and r^*, a supersonic Mach number is computed upstream of the throat, the computer will print "wrong solution—Mach should be less than 1." If a subsonic Mach number is computed downstream of the throat the computer will print "wrong solution—Mach should be greater than 1."

2. Temperature Ratios

$$\frac{T_0}{T} = 1 + \frac{\gamma-1}{2}M^2 \tag{35}$$

$$\frac{T_{aw}}{T_0} = \frac{1+0.89\frac{\gamma-1}{2}M^2}{1+\frac{\gamma-1}{2}M^2} \tag{18}$$

3. Constants in Integrals

$$a = \frac{T_w}{T} \tag{66}$$

$$b = \frac{T_0}{T_w} - 1 \tag{67}$$

$$c = \left(\frac{\gamma-1}{2}M^2\right)\left(\frac{T}{T_w}\right) \tag{68}$$

4. Flow Density

$$\rho U = \frac{(32.174/778.2)^{1/2}\,\gamma\, p_0 M}{[c_p T_0(\gamma-1)]^{1/2}\left(1+\frac{\gamma-1}{2}M^2\right)^{\frac{\gamma+1}{2(\gamma-1)}}} \tag{36}$$

The factor $(32.174/778.2)^{1/2}$ gives ρU the units of lbm/sec • in.^{2}

C. Equations for Iterative Simultaneous Solution of Momentum and Energy Equations

The equations in this Section are solved iteratively until the difference between successive values of ζ converges to RITE in a maximum of NO iterations, failing which the computer prints "zeta could not converge." The iteration yields the values of θ, ϕ, δ^*, C_f and C_h. An Adams-Moulton differential equation solver called "MARK" is employed. MARK is a machine language subroutine to PARK, a machine-language driver routine. A return to MARK from the derivative box is effected by CALL REMARK.

1. Momentum Equation

$$\frac{d\theta}{dz} = \frac{C_f}{2}\left[1+\left(\frac{dr}{dz}\right)^2\right]^{1/2} - \theta\left[\frac{2-M^2+\frac{\delta^*}{\theta}}{M\left(1+\frac{\gamma-1}{2}M^2\right)}\frac{dM}{dz}+\frac{1}{r}\frac{dr}{dz}\right] \tag{25}$$

2. Energy Equation

$$\frac{d\phi}{dz} = C_h\left(\frac{T_{aw} - T_w}{T_0 - T_w}\right)\left[1 + \left(\frac{dr}{dz}\right)^2\right]^{1/2} - \phi\left[\frac{1 - M^2}{M\left(1 + \frac{\gamma - 1}{2}M^2\right)}\frac{dM}{dz} + \frac{1}{r}\frac{dr}{dz} - \frac{1}{T_0 - T_w}\frac{dT_w}{dz}\right] \tag{30}$$

3. Reynolds Numbers

$$R_\theta = \left(\frac{12}{32.174}\right)\left(\frac{\rho U\theta}{\mu_0}\right)\left(1 + \frac{\gamma - 1}{2}M^2\right)^m \tag{34}$$

$$R_\phi = \left(\frac{12}{32.174}\right)\left(\frac{\rho U\phi}{\mu_0}\right)\left(1 + \frac{\gamma - 1}{2}M^2\right)^m \tag{45}$$

The factor 12/32.174 is required with the units employed in the program.

4. Skin-Friction Coefficient

a. Adiabatic skin-friction coefficient. For MPRO = 1, the following equations are solved iteratively by subroutine ADIABA, until the difference between successive values of C_{f_a} converges to 0.00001. For MPRO = 2 only $\bar{C}_f$ is computed.

$$\bar{C}_f\bar{R}_{\bar{\theta}} = \left(\frac{T_{aw}}{T}\right)^{1-m} C_{f_a}R_\theta \tag{43}$$

$$\bar{C}_f = \frac{0.009896}{(\bar{C}_f\bar{R}_{\bar{\theta}})^{0.562}} \qquad \bar{C}_f\bar{R}_{\bar{\theta}} \leqq 2.51 \tag{41}$$

$\bar{C}_f$ = linearly interpolated from Table 1 $\qquad 2.51 < \bar{C}_f\bar{R}_{\bar{\theta}} \leqq 64.8$

$$\left(\frac{2}{\bar{C}_f}\right)^{1/2} = 2.44\ln\left[\frac{\bar{C}_f\bar{R}_{\bar{\theta}}}{\bar{C}_f\left(3.781 - \frac{25.104}{(2/\bar{C}_f)^{1/2}}\right)}\right] + 7.68 \qquad \bar{C}_f\bar{R}_{\bar{\theta}} > 64.8 \tag{40}$$

$$\frac{T_s}{T_{aw}} = 1 + 17.2\left(\frac{T_0}{T_{aw}} - 1\right)\left(\frac{\bar{C}_f}{2}\right)^{1/2} - 305\left(\frac{T_0}{T_{aw}} - \frac{T}{T_{aw}}\right)\frac{\bar{C}_f}{2} \tag{39}$$

$$C_{f_a} = \frac{\bar{C}_f}{\left(\frac{T_{aw}}{T}\right)\left(\frac{T_s}{T_{aw}}\right)^m} \tag{42}$$

Equation (40) is solved by the regula-falsi method.

b. Diabatic skin-friction coefficient:

$$\frac{C_f}{C_{f_a}} = 1 \qquad \text{MPRO} = 1 \tag{31-a}$$

$$\frac{C_f}{\bar{C}_f} = \frac{1}{\left[\frac{1}{2}\left(\frac{T_w}{T} + 1\right)\right]^{(3-m)/4}} \qquad \text{MPRO} = 2 \tag{31-b}$$

5. Stanton Number

$$C_h = \frac{\frac{C_f(R_\phi)}{2}\left(\frac{\phi}{\theta}\right)^n}{1 - 5\left(\frac{C_f(R_\phi)}{2}\right)^{1/2}\left[1 - Pr + \ln\left(\frac{6}{5Pr + 1}\right)\right]} \tag{47}$$

6. Ratio of Displacement to Momentum Thickness

a. Case I, $\zeta \geqq 1$

$$\frac{\delta^*}{\theta} = \frac{\frac{a\zeta^7}{7} - I_2 - I_3}{I_1} \tag{82}$$

where

$$\zeta = \left[\frac{\phi I_1}{\theta\left(I_2' + \frac{I_3'}{\zeta}\right)}\right]^{1/8} \tag{83}$$

b. Case II, $\zeta < 1$

$$\frac{\delta^*}{\theta} = \frac{\frac{a}{7} - I_6 - I_7}{I_4 + I_5} \tag{93}$$

where

$$\zeta = \left[\frac{\phi(I_4 + I_5)}{\theta I_1'}\right]^{1/8} \tag{94}$$

Equations (83) and (94) are iterated for ζ by successive substitution. After the first three z-stations, a second-order extrapolation is employed to improve the initial guess.

D. Equations for Remaining Output Quantities

1. Velocity and Temperature Thicknesses

$$\frac{\theta}{\delta} = \frac{7}{a}I_1 \qquad \zeta \geqq 1 \tag{72}$$

$$\frac{\theta}{\delta} = \frac{7}{a}(I_4 + I_5) \qquad \zeta < 1 \tag{85}$$

$$\frac{\Delta}{\delta} = \zeta^7 \tag{65}$$

2. Heat-Transfer Coefficient

$$h_g = c_p \rho U C_h \tag{51}$$

3. Heat Flux

$$q_w = h_g (T_{aw} - T_w) \qquad \text{MPOT} = 1 \tag{52-a}$$

$$q_w = h_g \left(\frac{i_r - i_w}{c_p} \right) \qquad \text{MPOT} = 2 \tag{52-b}$$

4. Cumulative Heat Transfer

$$\text{SUMQ} = 2\pi \sum_{j=1}^{i} \frac{\Delta z}{2} \left\{ q_{w_j} r_j \left[1 + \left(\frac{dr}{dz} \right)_j^2 \right]^{1/2} + q_{w_{j-1}} r_{j-1} \left[1 + \left(\frac{dr}{dz} \right)_{j-1}^2 \right]^{1/2} \right\} \tag{53}$$

E. Integrals

Employing s as the dummy variable throughout:

$$I_1 = \int_0^1 \frac{s^7 (1 - s)}{1 + \frac{b}{\zeta} s - cs^2} ds \tag{73}$$

$$I_2 = \int_0^1 \frac{s^7}{1 + \frac{b}{\zeta} s - cs^2} ds \tag{76}$$

$$I_3 = \int_1^\zeta \frac{s^6}{1 + \frac{b}{\zeta} s - c} ds \tag{77}$$

$$I_4 = \int_0^\zeta \frac{s^7 (1 - s)}{1 + \frac{b}{\zeta} s - cs^2} ds \tag{86}$$

$$I_5 = \int_\zeta^1 \frac{s^7 (1 - s)}{1 + b - cs^2} ds \tag{87}$$

$$I_6 = \int_0^\zeta \frac{s^7}{1 + \frac{b}{\zeta} s - cs^2} ds \tag{89}$$

$$I_7 = \int_\zeta^1 \frac{s^7}{1 + b - cs^2} ds \tag{90}$$

$$I'_1 = \int_0^1 \frac{s^7 (1 - s)}{1 + bs - c\zeta^2 s^2} ds \tag{92}$$

$$I'_2 = \int_0^{1/\zeta} \frac{s^7 (1 - s)}{1 + bs - c\zeta^2 s^2} ds \tag{80}$$

$$I'_3 = \int_{1/\zeta}^1 \frac{s^6 (1 - s)}{1 + bs - c} ds \tag{81}$$

Gaussian integration is employed, utilizing the machine-language subroutine "GAL."

All subroutines and the main program are written to be assembled under the Fap-Fortran system. The format for fixed integers is 7I10 and for floating-point variables is 7F10.7. The $\bar{C}_f \bar{R}_{\bar{\theta}}$ vs $\bar{C}_f$ table must be placed directly behind the *DATA card and need be read in only once for single or multiple cases.